THE UNIVERSITY OF ARIZONA
University Libraries

UA CAMPUS REPOSITORY

Intracontinental subduction beneath the Pamir Mountains: Constraints from thermokinematic modeling of shortening in the Tajik fold-and-thrust belt

Item Type	Article
Authors	Chapman, James B.; Carrapa, Barbara; Ballato, Paolo; DeCelles, Peter G.; Worthington, James; Oimahmadov, Ilhomjon; Gadoev, Mustafo; Ketcham, Richard
Citation	James B. Chapman, Barbara Carrapa, Paolo Ballato, Peter G. DeCelles, James Worthington, Ilhomjon Oimahmadov, Mustafo Gadoev, Richard Ketcham; Intracontinental subduction beneath the Pamir Mountains: Constraints from thermokinematic modeling of shortening in the Tajik fold-and-thrust belt. GSA Bulletin ; 129 (11-12): 1450–1471. doi: https://doi.org/10.1130/B31730.1
DOI	10.1130/B31730.1
Publisher	GEOLOGICAL SOC AMER, INC
Journal	GEOLOGICAL SOCIETY OF AMERICA BULLETIN
Rights	© 2017 Geological Society of America.
Download date	26/08/2022 16:38:17
Item License	http://rightsstatements.org/vocab/InC/1.0/
Version	Final accepted manuscript
Link to Item	http://hdl.handle.net/10150/627829

Intracontinental subduction beneath the Pamir Mountains: constraints from thermokinematic modeling of shortening in the Tajik fold and thrust belt

James B. Chapman[1]
Barbara Carrapa[1]
Paolo Ballato[2]
Peter G. DeCelles[1]
James Worthington[1]
Ilhomjon Oimahmadov[3]
Mustafo Gadoev[3]
Richard Ketcham[4]

[1]Department of Geosciences, University of Arizona, Tucson, Arizona 85721, USA
[2]Department of Science, University of Rome Potsdam, Potsdam, Germany
[3]Institute of Geology, Earthquake Engineering and Seismology, Tajik Academy of Sciences, Dushanbe, Tajikistan
[4]Jackson School of Geosciences, University of Texas at Austin, Austin, Texas 78712, USA

Keywords: intracontinental subduction, Pamir; Tajik thrust belt;

Figures

1: Overview of Pamir
2: Tajik Basin Map
3. Cross Section across Tajik Basin
4. Flexural Model
5. Restored sections
6. Fetkin Results
7. Geothermal gradients plot
8. growth strata photo
9. cumulative shortening plot
10. alai, tarim, tajik basin schematic
11. Delamination model

Tables

Table 1: sample location, age, rock type, age overview
Table 2: Slip on major structures

Supplementary Material

File S1: matlab script

Table S1: Flexural model parameters
Table S2: AHe analyses
Table S3: AFT analyses

Figure S1: Bottom-hole temperature
Figure S2: Age-eU trends

ABSTRACT

A regional, balanced cross-section is presented for the thin-skinned Tajik fold and thrust belt (TFTB), constrained by new structural and stratigraphic data, industrial well-log data, flexural modeling, and existing geologic and geophysical mapping. A sequential restoration of the section is calibrated with 15 new apatite (U-Th)/He ages and 7 new apatite fission track ages from samples of the major thrust sheets within the TFTB. Thermokinematic modeling indicates that deformation in the TFTB began during the Miocene (≥ ~17 Ma) and continues to the near present with long-term shortening rates of ~4 to 6 mm/yr and Pliocene to present rates of ~6 to 8 mm/yr. The TFTB can be characterized as two distinct, oppositely verging thrust belts. Deformation initiated at opposite margins of the Tajik foreland basin, adjacent the southwest Tian Shan and northwest Pamir Mountains, and propagated toward the center of the basin, eventually incorporating it entirely into a composite fold-thrust belt. The western TFTB records at least 35-40 km of total shortening and is part of the greater Tian Shan orogenic system. The eastern TFTB records ~30 km of shortening that is linked to the Pamir Mountains. The amount of shortening in the TFTB is significantly less than predicted by models of intracontinental subduction that call for subduction of an ~300 km long slab of continental Tajik-Tarim lithosphere beneath the Pamir. Field observations and structural relationships suggest that the Mesozoic and younger sedimentary rocks of the Tajik Basin were deposited on and across the Northern Pamir terrane and then subsequently uplifted and eroded during orogenic growth, rather than subducted beneath the Pamir. The Paleozoic – Proterozoic (?) meta-sedimentary and igneous rocks exposed in the Northern Pamir terrane are equivalent to the middle-lower crust of the Tajik Basin, which has become incorporated into the Pamir orogen. We propose that the south-dipping zone of deep seismicity beneath the Pamir, which is the basis for the intracontinental subduction model, is related to gravitational foundering (by delamination or large-scale dripping) of Pamir lower crust and mantle lithosphere. This contrasts with previous models that related the Pamir seismic zone to subduction with or without roll-back of Asian lithosphere. Delamination may explain the initiation of extension in the Pamir gneiss domes and does not require a change in plate boundary forces to switch between compressional and extensional regimes. Because the Pamir is the archetype for active subduction of continental lithosphere in the interior of continental plates (intracontinental subduction), the viability of this particular tectonic processes may need to be reassessed.

INTRODUCTION

The Pamir region is the most prominent and widely-cited example of intracontinental subduction in the world (Roecker et al., 1982; Hamburger et al., 1992; Burtman and Molnar, 1993; Fan et al., 1994; Pavlis et al., 1997; Kumar et al., 2005; Negredo et al., 2007; Mechie et al., 2012; Schneider et al., 2013;

Sippl et al., 2013; Sobel et al., 2013; Kufner et al., 2016). The intracontinental subduction model suggests that the Pamir has advanced ~300 km over its foreland, the Tajik-Tarim Basin, and that Asian continental lithosphere is subducted beneath the Pamir, forming a "Pamir slab" that generates deep seismicity (Burtman and Molnar, 1993; Mechie et al., 2012; Schneider et al., 2013; Sippl et al., 2013) (Fig. 1). In some versions of this model, Asian lower crust and mantle lithosphere is first underthrust or subducted at a low-angle beneath the Pamir and then rolls back northward (Sobel et al., 2013). Other hypotheses for the origin of the Pamir slab include aspects of subduction, underthrusting, roll-back, foundering, and forced-delamination (Stearns et al., 2015; Kufner et al., 2016; Rutte et al., 2017b). A straightforward test of the intracontinental subduction model can be accomplished by quantifying the amount and timing of shortening in the Northern Pamir and Tajik fold and thrust belt (TFTB). The intracontinental subduction model predicts ~300 km of Cenozoic shortening, which is the approximate down-dip length of the Pamir "slab" as seismically imaged in the mantle (Burtman and Molnar, 1993; Bourgeois et al., 1997; Burtman, 2000; Schneider et al., 2013; Sippl et al., 2013). Structural reconstructions of the Pamir slab indicate it may be as long as 380 km (Rutte et al., 2017b).

In order to test the intracontinental subduction model in the Pamir, a structurally balanced cross-section across the TFTB and Northern Pamir is presented along with new apatite (U-Th)/He (AHe) and apatite fission track (AFT) thermochronological ages collected from major structures within the TFTB. Structural and thermochronologic data are combined in a thermokinematic model that produces synthetic thermochronologic ages based on a sequence of partially restored cross-sections. This modeling provides constraints on the geometry, magnitude of deformation, timing of deformation, and structural evolution of the TFTB. The results suggest that >50% of the shortening in the TFTB is related to Miocene and younger convergence between the Tian Shan and Tajik-Tarim lithosphere. The remaining shortening in the TFTB (~30 km) is significantly less than the ~ 300 km of shortening required by models of subduction of Tajik continental (Asian) lithosphere. We advocate an alternate explanation in which the Pamir lower crust and mantle lithosphere have delaminated or foundered as a result of internal orogenic thickening and potential eclogitization (Fig. 1C). Although the kinematics of roll-back of previously subducted Asian lithosphere and delamination of thickened Pamir lithosphere may be similar (Sobel et al., 2013; Stearns et al., 2015; Kufner et al., 2016; Rutte et al., 2017b), the driving mechanisms are distinct and have important implications for: 1) the feasibility of continental subduction in the Pamir; 2) whether subduction can occur outside of plate margins; 3) the long-term evolution of convergent orogenic plateaus, and 4) the relationship between contemporaneous deformation in the upper crust, lower crust, and mantle lithosphere. It is important to distinguish between subduction-related processes like roll-back, which are driven by the dynamics of the slab or lower plate (Schellart, 2008) and delamination of thickened orogenic roots, which is a function of upper plate processes (Bird, 1979) that do not necessarily need to be mechanically or kinematically coupled to the subducting plate (DeCelles et al., 2009; 2015). Subduction, including flat-slab subduction, is driven by forces acting on the lower plate (e.g., slab pull, ridge push, mantle traction) (Forsyth and Uyeda, 1975), whereas underthrusting (low-angle thrust faulting) within the interior of a continent is driven by forces acting on the upper plate (e.g., plate boundary, gravitational).

REGIONAL GEOLOGY

Tian Shan

The Tian Shan consists of a collection of terranes that were accreted to Eurasia during the Paleozoic (Windley et al., 1990). The Tian Shan was reactivated during the Cenozoic in response to India-Asia collision (Tapponnier and Molnar, 1979). Uplift and exhumation of the Central Tian Shan began during the late Oligocene to early Miocene (Hendrix et al., 1994; Sobel and Dumitru, 1997; Sobel et al., 2006; Heermance et al., 2008) and cooling ages near the Alai Valley (Fig. 1) indicate that denudation of the southwestern Tian Shan may have also begun during the early Miocene (20-22 Ma) (DeGrave et al., 2012, Sobel et al., 2013). Deformation progressed into thin-skinned foreland thrust belts south of the Central Tian Shan during the middle to late Miocene (Yin et al., 1998; Heermance et al., 2008; Fu et al., 2010) in response to underthrusting of Tarim continental lithosphere (Roecker et al., 1993; Allen et al, 1999; Scharer et al., 2004; Makarov et al., 2010). The southern margin of the Tian Shan consists of several thin-skinned fold and thrust belts including the Kashi, Kepintage, and Kuqa (a.k.a. Kuche) segments (Fig.1). These thrust belt segments experienced 10-40 km of shortening during the Miocene and shortening rates have accelerated during the last 2-4 Ma (Scharer et al., 2004; Chen et al., 2007; Heermance et al., 2008; Yin et al., 1998; Allen et al., 1999; Sun et al., 2009). In this contribution, we will make a direct comparison between the style, magnitude, and timing of deformation in the western TFTB and the thrust belts bordering the southeast margin of the Central Tian Shan orogenic system.

Pamir

The Pamir consists of the Northern, Central, and Southern Pamir terranes (Burtman and Molnar, 1993). These three terranes, and the Pamir in general, are regarded as the westward prolongation of the Tibetan Plateau. The Northern Pamir terrane is equivalent with the Kunlun terrane and the Central and Southern Pamir terranes are equivalent with the Qiangtang terrane (Robinson et al., 2012). The Northern Pamir terrane comprises the Kunlun magmatic arc and the Karakul-Mazar arc-accretionary complex, which are part of a Cordilleran-style margin that formed the southern continental edge of Central Asia during Carboniferous to Triassic time (Schwab et al., 2004) (Fig. 1). The Central and Southern Pamir terranes were accreted to Asia during the early Mesozoic (Burtman and Molnar, 1993; Schwab et al., 2004; Robinson et al., 2012; Angiolini et al., 2013). The sutures between the Northern, Central, and Southern Pamir terranes appear to be deflected northward and wrap around the Pamir salient (Fig. 1). The geometry of these sutures has been used to suggest that the Pamir were thrust northward across the Tajik-Tarim Basin (Burtman and Molnar, 1993). Other geological evidence mustered for the northward displacement of the Pamir salient are paleomagnetic vertical-axis rotations (Bazhenov and Burtman, 1986; Pozzi and Feinberg, 1991; Bosboom et al., 2014) and Cenozoic shortening within the Pamir and TFTB (Burtman and Molnar, 1993). Internal shortening within the Pamir during the Cenozoic has been estimated at 80 to >95 km (Robinson, 2015; Rutte et al., 2017a), which is less than the ~300 km of internal shortening suggested by Burtman and Molnar (1993). Regardless, if the Tajik-Tarim lithosphere is subducting beneath the Pamir, then the amount of internal shortening in the upper plate (Pamir Mountains) is not indicative of the amount of subduction (slab length) in the lower plate. The length of subducted Tajik-Tarim lower crust and mantle lithosphere should balance the amount of shortening in upper crust of the Tajik-Tarim lithosphere (e.g. Tajik Basin), not the Pamir. Detrital thermochronology of modern sands from the rivers draining the western Pamir suggests that exhumation started in the late Oligocene to early Miocene (20-25 Ma) (Lukens et al., 2012; Carrapa et al. 2014). These results are consistent with significant topography and regional erosion and with the timing for tectonic exhumation of the Pamir gneiss domes (Stearns et al., 2013; 2015). There are no bedrock thermocrhonological ages in the western part of the north Pamir outside of the gneiss domes, although Amidon and Hynek (2010) and Sobel et al. (2013) report low-temperature cooling ages as young as early Miocene for the northwestern Pamir margin, approximately 200 km from the line of the cross-section presented in this study.

In addition to the geological evidence, several geophysical studies have suggested that the Pamir is thrust over the Tajik-Tarim Basin. The Pamir sits above two oppositely inclined zones of intermediate-depth seismicity. Beneath the westernmost Pamir, the Hindu Kush seismic zone dips steeply northward, whereas across the rest of the Pamir, the Pamir seismic zone dips steeply southward. Tomographic and receiver function studies have indicated the presence of a low-velocity layer within these seismic zones, suggesting that they may include a component of continental crust (Roecker, 1982; Koulakov and Sobolev, 2006; Schneider et al., 2013; Sippl et al., 2013). These seismic zones have been interpreted as: (1) remnant pieces of oceanic lithosphere with a small component of Indian crust attached (Pegler and Das, 1998; Pavlis and Das, 2000), (2) Indian continental lithosphere (Roecker, 1982; Koulakov and Sobolev, 2006), (3) subducted Asian continental lithosphere (Schneider et al., 2013; Sippl et al., 2013), or (4) a combination of subducting Indian lithosphere in the Hindu Kush seismic zone and subducting Asian lithosphere in the Pamir seismic zone (Hamburger et al., 1992; Burtman and Molnar, 1993; Fan et al., 1994; Pavlis et al., 1997; Burtman, 2000; Kumar et al., 2005; Negredo et al., 2007; Mechie et al., 2012;

Kufner et al., 2016). The south-dipping Pamir seismic zone extends ~250 km into the mantle and projects up-dip toward the Main Pamir Thrust (MPT) and Pamir Frontal Thrust (PFT), an active fault zone at the surface located in the Alai Valley between the Pamir and Tian Shan (Figs. 1, 2). Focal-mechanisms (Fan et al., 1994), structural studies (Pavlis et al., 1997; Coutand et al., 2002), neotectonic markers (Strecker et al., 2003; Thompson et al., 2015), and GPS measurements (Mohadjer et al., 2010; Ischuk et al., 2013) indicate that the northern margin of the Pamir is actively accommodating convergence.

Tajik Basin

The Tajik Basin is underlain by continental crust that was accreted to the southern Eurasian margin during late Carboniferous to early Permian time (Burtman and Molnar, 1993, Schwab et al., 2004; De Grave et al., 2012; Schneider et al., 2013). No rocks older than the Jurassic are exposed within the Tajik Basin, but Permian and Triassic sedimentary rocks are locally present along the basin margins and increase in thickness eastward and southward (Nikolaev, 2002) (Fig. 2). The Tajik Basin crust is interpreted to have experienced limited Triassic extension, which may give rise to east-west oriented basement structures (Leith, 1985; Thomas et al., 1994; Brookfield and Hashmat, 2001; Nikolaev, 2002). Regional, basin-wide deposition began during the early Jurassic with nonmarine conglomerates and coal that transition to shallow marine carbonate rocks and eventually evaporites in the upper Jurassic (Brookfield and Hashmat, 2001). Upper Jurassic evaporite facies in the Guardak Formation are an important décollement level within the TFTB (Thomas et al., 1994; Bekker, 1996). During Cretaceous through Paleogene time, the axis of the Tajik Basin trended approximately east-west and shallow marine to nonmarine clastic facies were deposited. Numerous fluctuations in relative sea-level produced minor disconformities (Burtman, 2000; Nikolaev, 2002). Foreland basin subsidence associated with growth of the Pamir started no later than Eocene time (Leith, 1985; Carrapa et al., 2015). Sediment grain size increased through the Oligocene and culminated with deposition of thick, coarse-grained conglomerates during the Miocene (Coutand et al., 2002; Nikolaev, 2002; Klocke et al., 2015).

Tajik Fold and Thrust Belt

The TFTB consists of a series of thrust faults and folds that roughly parallel the margin of the Pamir salient (Fig. 2). Structures in the east half of the TFTB verge toward the Tian Shan, structures in the west half of the TFTB verge toward the Pamir, and the intervening middle of the thrust belt forms a large synclinorium in the Yovon Valley (Thomas et al., 1994; Bekker, 1996; Bourgeois et al., 1997) (Fig. 3). This contrasts sharply with typical thrust belts in which thrusts predominantly verge toward the foreland (Bonini, 2007). Some researchers have hypothesized that the east-verging structures in the western TFTB are backthrusts near the toe of a thrust belt that is kinematically linked to growth of the Pamir (Leith and Alvarez, 1985; Reiter et al., 2011).

Total shortening in the TFTB across the Tajik Basin has been reported to be as much as 300 km, which includes shortening across the southwest Gissar Range (Burtman and Molnar, 1993; Bourgeois et al., 1997; Burtman, 2000). Shortening estimates between the Pamir and the Tian Shan in the Peter the First Range (~60 km) (Hamburger et al., 1992) and Alai Valley (~16 km) (Coutand et al., 2002) are significantly smaller than the reported shortening in the Tajik Basin (Thomas et al., 1994; Bourgeois et al., 1997) (Fig. 1). Paleomagnetic data indicate counterclockwise vertical axis rotations of up to 50 degrees in the TFTB (Bazhenov and Burtman, 1986; Thomas et al., 1994) and some researchers have also suggested that many of the currently north-south trending structures in the TFTB were oriented northeast-southwest or east-west prior to the indentation of the Pamir salient (Burtman and Molnar, 1993; Bourgeois et al., 1997; Burtman, 2000).

Initiation of deformation in the TFTB is poorly constrained, mainly owing to a lack of age control on synorogenic sedimentary rocks (Klocke et al., 2015). An undeformed foreland basin occupied the present Tajik basin in the Paleogene (Carrapa et al., 2014) suggesting that incorporation of the foreland into the wedge-top and fold and thrust belt started post Oligocene time. Nikolaev (2002) suggested Oligocene-age growth strata in the TFTB, and Burtman (2000) proposed that deformation in the interior of the TFTB began during the Pliocene. Some studies have hypothesized that the TFTB may have initiated in the Miocene as a result of gravitational collapse of the Pamir (Stübner et al., 2013; Rutte et al., 2017b). The TFTB is still active today and GPS measurements indicate ~5-10 mm/yr convergence across the TFTB in a northwest-southeast direction (Mohadjer, 2010; Ischuk et al., 2013). Apart from sparse biostratigraphic data (Wang et al., 2013), our thermochronological results provide some of the first constraints on the timing of exhumation and deformation in the TFTB.

METHODS

Cross-Section Construction and Restoration

We built two cross-sections: 1) cross-section A-A', a regional, ~350 km long, balanced cross-section that crosses the southwest Gissar Range in Uzbekistan, the central Tajik Basin and TFTB in Tajikistan, and ends within the Northern Pamir terrane in Afghanistan, and 2) cross-section B-B', a ~100 km long, balanced cross-section that starts in the Southern Tian Shan, crosses the Peter 1st Range, Northern Pamir terrane, and ends near the suture between the Northern and Central Pamir terranes in Tajikistan (Figs. 2, 3). Cross-section A-A' was constructed by combining our observations with previous geologic mapping (Vlasov et al., 1991), new structural and stratigraphic data collected in the 2014 and 2015 field seasons, well-log data provided by a grant from TGS-NOPEC Geophysical Company, and depth-to-basement maps generated from gravity, magnetic, and refraction seismic data (Nikolaev, 2002). The orientation of the cross-section is sub-orthogonal to fold axes within the TFTB and parallel to the inferred tectonic transport direction (e.g., Boyer and Elliott, 1982); we assume plane strain and incompressibility (e.g., Judge and Allmendinger, 2011). Paleomagnetic data indicate that fault-slip on individual structures may increase to the northwest (Bourgeois et al., 1997), but we do not observe any out-of-plane component of displacement along the length of our section. Apparent dips were calculated from surface data and projected onto the section line. Structural and well data were perpendicularly projected onto the plane of section from up to 5 km and 20 km away, respectively (Fig. 2). No attempt was made to incorporate deformation at a scale below ~1 km. Where unknown, thrust fault names were assigned based on the names of the mountain ranges in the hangingwall. Hangingwall cut-off positions that have passed through the erosion surface were constructed using conservative geometries that minimize fault offset and shortening. No penetrative deformation was observed in the Mesozoic and younger sedimentary cover and flexural slip and line-length balancing methods were used to restore the section by hand and with Midland Valley's Move software. Field observations support the use of concentric fold geometry. Estimates of shortening are based on line length restoration of Cretaceous and younger stratigraphic contacts (e.g., Bally et al., 1966; Dahlstrom, 1969; Price and Mountjoy, 1970; Hossack, 1979; Woodward et al., 1989; Judge and Allmendinger, 2011).

Cross-section B-B' is located close to the plane of the cross-section presented in Hamburger et al. (1992) that crossed the PFT (Fig. 3). The geometry of the PFT was adopted from Hamburger et al. (1992) and the cross-section was extended into the Pamir to illustrate the geometry of the Mesozoic to Cenozoic sedimentary rocks and the MPT. It is constrained by surface structural data and previous geologic mapping (Vlasov et al., 1991, Hamburger et al., 1992) and was constructed and restored using the same techniques described above. Igneous intrusions in both cross-section A-A' and B-B' are not shown because they obscure structural relations.

Flexural and Subsidence Modeling

Cross-section A-A', combined with previous geophysical studies, indicates significant structural relief on the upper Jurassic décollement (Fig. 3a). At least part of this relief may be related to flexure of the Tajik Basin lithosphere in response to loading by the Tian Shan and Pamir Mountains. To estimate the potential role of these loads, flexure of the Tajik Basin lithosphere was modeled in two-dimensions using a centered finite-difference technique that solves the flexural equations of Turcotte and Schubert (2014) (Fig. 4). Using a numerical model, rather than an analytical solution, allows flexural rigidity to vary spatially across the Tajik Basin. First, the thickness of the pre-Miocene section in the central Tajik Basin (~3.3 km) was added to the depth of the décollement to model the flexural deflection from zero elevation. Next, the geometry of the modern décollement (Fig. 3) was approximated with a flexural profile using a flexural rigidity of 5×10^{22} for the region west of Yovon valley and 1×10^{22} Nm east of Yovon valley (Fig. 4). The loads used are 2 km (height) × 200 km (width) rectangular blocks with a density of 2700 kg/m^3, each centered on the Pamir and Tian Shan mountain fronts. The modern topographic relief between the Tajik Basin and the western Pamir or SW Gissar range is also ~2 km.

The heights of the loads were progressively reduced for each partially restored cross-section to simulate flexural subsidence. Load height was reduced by 150 m/Myr from 0 Ma to 8 Ma and by ~ 65 m/Myr from 8 Ma to 20 Ma. These rates were chosen to match the observed thicknesses of Miocene and younger sedimentary rocks (Nikolaev, 2002). No correction was made for sediment compaction and the load position, density, and horizontal extent did not change through time. A MATLAB script containing the model and a table with detailed information on the flexural parameters for each time step is presented in the supporting information (File S1, Table S1). Although this approach does not rigorously relate thrust belt kinematics to foreland subsidence and deposition (e.g., Robinson and McQuarrie, 2012), it does broadly capture changes in subsidence as recorded by measured sediment thicknesses and makes predictions for how the geometry of the Jurassic décollement may have changed through time in response to flexure.

Low-Temperature Thermochronology

To constrain the timing of deformation and the pattern of thrust propagation within the TFTB, samples were collected for apatite fission track (AFT) and apatite (U-Th)/He (AHe) thermochronology (Table 1) along the trace of cross-section A-A'. These techniques allow determination of the ca. 120°C - 40°C temperature-time history of the sample, which encompasses the temperature range of the AHe partial retention zone (~ 40°C - 80°C) and AFT partial annealing zone (~ 80°C - 120°C) (Green and Duddy, 1989; Farley, 2002; Reiners and Brandon, 2006). Assuming that cooling was associated with displacement of hangingwall rocks and erosion, cooling ages can be used as a proxy for deformation (Lock and Willet, 2008; Carrapa et al., 2011). Eleven Lower Cretaceous sedimentary rocks (the oldest clastic unit exposed in the Tajik Basin) were analyzed from the hangingwall of each of the major thrust sheets and from the crests of major detachment folds. One Lower Cretaceous sandstone and one Lower Jurassic sandstone from the Dashtijum Valley region were also analyzed (Fig. 2). Additionally, two samples of Neogene sandstone from the footwall of the Bobotogh thrust and the Aruntau thrust were analyzed (Fig. 3). All samples were collected from near the same elevation in the Tajik Basin, ranging from 700-1300 m. For AFT analysis, apatites were separated, mounted, and etched in 5.5 M nitric acid for 20s at 21°C according to the protocols of Donelick et al. (1999; 2005). Fission track ages were calculated using the external detector method (Hurford and Green, 1983). Irradiation was performed at the Oregon State University reactor. After irradiation, the mica prints were etched in 49% hydrofluoric acid for 15 minutes at 23°C following Donelick et al. (1999; 2005) and analyses were conducted at the University of Arizona Fission Track Laboratory. AHe analyses were performed at the University of Arizona (U-Th-[Sm])/He Laboratory following the methods described in Reiners et al. (2004).

Thermokinematic Modeling

To constrain the geometry and kinematic evolution of the TFTB, thermochronological ages were forward modeled using FETKin (Finite Element ThermoKinematic modeling). FETKin is a computer program that solves the advection-diffusion equation for heat in two dimensions using the finite element method (Almendral et al., 2015). The primary inputs into FETKin are a series of displacement vector fields for each partially restored cross-section, topography, a fixed temperature at the base of the model, and heat production. The primary outputs of FETKin are calculated time-temperature paths, isotherms, and thermochronometer ages. FETKin cooling ages are calculated from time-temperature paths, in a forward sense, using the same algorithms as the thermal history modeling program HeFTy (Ketcham, 2005; Ketcham et al., 2007). Models were evaluated by how well the predicted thermochronometer ages match observed thermochronologic data and how well predicted geothermal gradients matched the modern geothermal gradient. Details of a typical FETKin workflow can be found in Mora et al. (2015).

After building and retro-deforming cross-section A-A' to ensure it balanced, the fully-restored geometry of the TFTB was simplified to aid in the modeling process. Faults were modeled as planar ramps and flats. The restored-state cross-section was then forward modeled to simulate progressive deformation through a series of 2 Myr time steps, from 20 Ma to 0 Ma, spanning the range of ages in the thermochronological dataset (Fig. 5). Fault-parallel-flow and detachment fold algorithms were used within MOVE for the forward modeling. The final geometry and magnitude of cumulative slip on individual faults in the present-day modeled section was required to match the present-day cross-section (Fig. 3). For all other time steps, the magnitude of slip on individual faults or folds was varied in an iterative process until the synthetic cooling ages predicted by FETKin converged on the measured (observed) cooling ages (Fig. 6).

The final (0 Ma time step) model geometries are shown in Figure 6 and only cover the parts of the cross-section for which reliable thermochronological cooling ages are available. The FETKin finite element grid in all model runs was 225 km wide and 25 km deep with 1 km node spacing in both dimensions. Model topography was kept flat and constant with an elevation equal to the mean elevation in the Tajik Basin (~800m). The surface temperature was kept constant at 15 °C. All models use constant thermal conductivity of 0.25 W/(m K), constant rock density of 2500 kg/m^3, and constant specific heat of 1000 J/kg °C.

All model runs begin with model nodes prescribed an inherited age. Experimentation with different inherited ages showed little effect on the final reset or partially reset ages in the model. Therefore, 30 Ma was prescribed as a uniform inherited age in order to easily show synthetic inherited and partially reset ages on the same plot (Fig. 6). The thermochronological samples are all sandstones and the true inherited age for each grain is not known so that it is impossible to precisely model partially reset ages without additional information. However, the similarities between AFT and AHe ages suggest that the samples cooled relatively rapidly through the respective closure temperature windows.

The topographic relief between adjacent ridgetops and valleys in the Tajik Basin is everywhere < 1 km, commonly < 0.5 km, and most of the valleys in the Tajik Basin are actively accumulating sediment. Undated growth strata on structures in the TFTB indicate contemporaneous fault slip, erosion, and deposition. No evidence of significant normal faulting exists in the Tajik Basin. The range in thermochronological cooling ages across the Tajik Basin (including unreset ages in valleys) indicates that the calculated cooling ages are not a result of a basin-wide erosional event. For these reasons, we assert that exhumation and cooling were caused by erosion in response to deformation-related rock uplift.

The modern geothermal gradient for the Tajik Basin was estimated by plotting bottom-hole temperatures recorded in wells in the Tajik Basin against the total depth of the wells (supporting information Figure S1). Linear regression of these data was anchored to a y-intercept of 18°C, which is the approximate modern mean annual surface temperature for the Tajik Basin area (temperature data from the National Oceanic and Atmospheric Administration, www.ncdc.noaa.gov). The regression indicates a modern geothermal gradient of ~22 °C/km. Temperatures recorded in boreholes are generally considered minimum temperatures because drilling fluids pumped from the surface tend to cool the borehole and may be mixed with formation fluids (Bullard, 1947). Therefore, the modern geothermal gradient is estimated at 22 - 25 °C/km.

Geothermal gradients in FETKin (calculated from model isotherms) are controlled by the basal temperature, the advection of material through the erosion surface (by rock uplift or sediment deposition), and radiogenic heat production. Heat production can significantly change predicted cooling ages if the synthetic sample is close to the closure temperature for the relevant thermochronometer (Whipp et al., 2006; McQuarrie and Ehlers, 2015). Average heat production for continental crust is ~0.9 μW m^{-3} (Rudnick and Gao, 2003; Mareschal and Jaupart, 2013), with high heat production (> 1.0 μW m^{-3}) in the uppermost crust (≤ 10-15 km depth) that rapidly decreases to lower values (≤ 0.5 μW m^{-3}) in the lower crust (Ketcham, 1996; Brady et al., 2006). We could not find heat production data from the Tajik Basin, but data from the Tarim Basin indicate that radiogenic heat production in Mesozoic to Cenozoic sedimentary rocks (at the surface or in boreholes) is ≤ 1.2 μW m^{-3} (Qui et al., 2012). Although not ideal, the current version of FETKin employs a constant heat production value throughout the model that competes with the basal temperature of the model to determine geothermal gradient. There is a natural trade-off between heat production and basal heat flow in thermokinematic models such that similar isotherms can be generated by increasing heat production and reducing basal heat or vice versa (Coutand et al., 2014; Erdos et al., 2014; McQuarrie and Ehlers, 2015). In the suite of models presented below, the effect of increasing heat in the system is evaluated by varying basal temperature in the model and setting heat production to zero. Model geothermal gradients were calculated at each location in the model by regressing a line through the upper 10 km of model isotherms at that location (Fig. 7). This avoids isotherm perturbations that are caused by the fixed (horizontal isotherm) basal temperature. None of the modeled tsamples was exhumed from or buried to a depth > 10 km.

RESULTS

The Tajik Fold and Thrust Belt

Similar to previously published cross-sections across the Tajik Basin (Thomas et al., 1994; Bourgeois et al., 1997), cross-section A-A’ shows bivergence toward the center of the basin. Based on this bivergence, the TFTB is separated into the east-vergent West TFTB and the west-vergent East TFTB. The hinterland regions for these thrust belts are the southwest Gissar Range and the Pamir, respectively.

The Southwest Gissar Range

The southwest Gissar Range in the southwest Tian Shan includes three large basement-involved reverse faults that verge to the east and one reverse fault that verges to the west (Fig. 2, 3). We define basement in the southwest Tian Shan as Early Permian and older rocks, which are primarily Early Permian igneous rocks and penetratively deformed Carboniferous and older metasedimentary rocks that were metamorphosed during the collision of the Tian Shan and Tajik-Tarim craton (Kässsner et al., 2016). Based on previous geologic mapping and the cross-section reconstruction of Mesozoic and younger strata (Fig. 3), 20-25 km of shortening are estimated across the southwest Gissar Range. The structure of the southwest Gissar Range at depth is unknown. One of many viable geometric possibilities is presented that allows the regional cross-section to balance (Fig. 3a). Other possibilities include a series of duplexes or a mid-crustal detachment. Equal-area balancing methods (Mitra and Namson, 1989) on Upper Cretaceous strata indicate the folding observed at the surface in the southwest Gissar Range could be balanced by a horizontal detachment at ~15 km depth. The structural interpretation for the Gissar Range suggests that uplift of the southwest Gissar Range was accomplished in part by underthrusting of the middle to lower crust of Tajik Basin, which is balanced by shortening in the West TFTB (Fig. 3).

West Tajik Fold and Thrust Belt

In the West TFTB, the Bobotagh thrust fault is the first major thin-skinned structure east of the Tian Shan front (Fig. 3). Thin layers of evaporite and sandstone, interpreted to be Jurassic in age, are locally exposed along the fault trace and appear to be unconformably (10-20° angular discordance) overlain by the Cretaceous section. A major décollement is inferred in evaporite facies of the upper Jurassic Guardak Formation that the Bobotogh thrust, and all other major thrust faults in the TFTB, sole into at depth. Lower Cretaceous strata at the base of the Bobotogh thrust sheet dip 35-45° NW, which is interpreted to indicate the dip of the underlying frontal thrust ramp. This dip angle is nearly constant throughout the Cretaceous and lower Paleogene section. Cenozoic sedimentary rocks overlie in angular unconformity lower Paleogene strata along the west side of Bobotogh Ridge (Fig. 3). Bedding in the Cenozoic section dips to the northwest at angles decreasing upsection from 25° to 5°, recording growth of the Bobotogh structure (Fig. 3). Based on age assignments from Soviet-era geologic mapping (Vlasov et al., 1991) and sparse mammalian fossils (Wang et al., 2013), these growth strata record deformation during Oligo-Miocene time. The reconstruction suggests a minimum of 12.5 km of slip on the Bobotogh thrust.

Cenozoic strata in the footwall of the Bobotagh thrust fault are significantly steeper with dips up to 75° on the northwest limb of a large hangingwall anticline in the Karshi thrust sheet (Fig. 3). We interpret the steep dips to result from progressive rotation of the Karshi thrust sheet during emplacement of additional structurally lower thrust sheets to the southeast. The moderate dip of bedding in the Bobotogh thrust sheet contrasts with the steeply dipping Cenozoic to Mesozoic strata in the Karshi thrust sheet. These field relationships suggest that at least part of the slip on the Bobotogh thrust post-dates movement on the Karshi thrust. The hangingwall anticline in the Karshi thrust plunges northeastward, which provides a constraint on hangingwall cut-off positions and slip estimates. The reconstruction suggests ~8 km of slip on the Karshi thrust.

The next three thrust faults east of the Karshi thrust are the Rangon, Aruntau, and Jetimtau thrusts. Rocks in the hangingwalls of each of these thrust sheets are folded into large concentric anticlines, the backlimbs of which dip toward the northwest. The northwest dipping panels are inferred to result from the shapes of the underlying thrust ramps (Fig. 3), and the general southeastward decrease in backlimb dip of each of these three thrust sheets corresponds to a forward-breaking, southeastward progression of thrust sheet emplacement (i.e., footwall imbrication). There is no hangingwall cut-off constraint for the Rangon thrust and slip is conservatively estimated at ~6 km. Hangingwall anticlines and cut-off positions are preserved along strike for both the Aruntau and Jetimtau thrust sheets. Estimates of slip based on the structural reconstruction for these two faults are ~6 km and ~ 7 km respectively. The presence of hangingwall cut-offs in Cretaceous to Cenozoic strata indicates that these thrust faults can each be considered a single frontal ramp that merges with the bedding-parallel Jurassic décollement. In total, there is 35-40 km of shortening recorded in the West TFTB (Fig. 3).

East Tajik Fold and Thrust Belt

Separating the West TFTB and East TFTB is the 20-25 km wide Yovon Valley (Figs. 2, 3). The East side of Yovon Valley is bounded by the west-vergent Karatau thrust fault with evaporitic rocks locally exposed along the fault trace. A large hangingwall anticline in the Karatau thrust sheet plunges to both the north and south, preserving hangingwall cut-offs (Fig. 2). The reconstructed section suggests ~7 km of fault slip and ~2 km of detachment fold-related shortening in the Karatau thrust sheet (~9 km of total shortening). North of the Karatau thrust sheet a west-verging hangingwall anticline plunges beneath the Yovon Valley with no surface expression at the latitude of the cross-section. This structure is represented schematically beneath the Yovon Valley on the cross-section (Fig. 3).

Sandwiched between the Karatau thrust sheet and the Sarsarak thrust sheet to the east is the Vakhsh River (Fig. 2), one of the largest rivers in Tajikistan. Sub-vertically dipping slivers of upper Cretaceous to lower Paleogene strata are exposed in the Vakhsh River Valley and likely represent minor thrust flats or small duplex systems. The Sarsarak thrust fault locally cuts down-section in the transport direction into older rock units within the Karatau thrust sheet, which strongly suggests that at least some movement on the Sarsarak thrust post-dates the formation of the Karatau anticline (Fig. 3). Furthermore, the structural relief of the Sarsarak thrust sheet requires structural duplication or thickening at depth, which can readily be accomplished with a footwall thrust flat (Fig. 3). The corresponding hangingwall flat would have been eroded by the Vakhsh River and can help to explain the absence of middle Paleogene and younger rocks in the Vakhsh River Valley. The reconstruction suggests ~4 km of slip on the Sarsarak thrust fault.

Structurally above and east of the Sarsarak thrust sheet is the Sangyaak thrust, which is exposed north of the plane of section, near the town of Nurek where it is west-verging. The Sangyaak thrust tips out to the south within the core of the upright Sangyaak anticline, rather than in a synclinal limb or at the base of a hangingwall anticline (Fig. 2). This fault-fold relationship is indicative of a faulted detachment fold (Mitra, 2002). The along-strike exposure suggests that the Sangyaak structure initially formed as a detachment fold that was eventually broken by a thrust fault with continued shortening. This structural style is characteristic of most of the East TFTB and characterizes the Vakhsh thrust, which also tips out to the south in a detachment fold (Fig. 2). We estimate 1.5 km of slip on the Sangyaak detachment fold and 4 km of slip on the Vakhsh detachment fold/thrust in the plane of the cross-section.

East of the Vakhsh detachment fold and west of the Dashtijumb Valley, the landscape consists of vegetated grassland and farmland characterized by bucolic rolling hills and poor exposure. Most of this landscape appears to be covered by unconsolidated loess deposits of unknown age. This area was not examined in detail and the cross-section relies on previous geologic mapping and sparse well-data. Previous mapping of Neogene strata in this region suggests a series of upright, gentle folds with wavelengths of 15-25 km (Vlasov et al., 1991). The axes of these folds trend northeastward, toward the Peter the First Range, where deeper structural levels reveal a series of tight detachment folds in the Mesozoic section (Hamburger et al., 1992). The interpretation at depth in this region is based on the more tightly folded Mesozoic rocks along strike and suggests that much of the Neogene section at the surface is composed of growth strata with relatively lower dip angles.

Dashtijum Valley: The Pamir Foothills

The Dashtijum Valley region contains a large overturned syncline (Fig. 3). The corresponding anticline that shares the overturned fold limb has been eroded, but must have had an amplitude of > 5 km assuming line-length balancing and constant bed thickness in the eroded section (Fig. 3; Cross-section A-A'). Bedding in the Mesozoic section is overturned and dips 55° to 65° E. The Paleogene section is also overturned with bedding dipping 65° to 90° E. Bedding becomes upright in the Miocene (?), and progressively flattens up-section. The Miocene (?) and younger rocks in the east limb of the large overturned syncline contain growth strata that record progressive westward tilting of bedding (Fig. 3, 8), presumably associated with growth of the overturned syncline and/or structural thickening at depth.

The topographic expression of the Dashtijum Valley follows the surface exposure of upper Jurassic evaporites in the Guardak Formation. These evaporites are locally exposed along both sides of the valley floor and display bedding that dips steeply to vertical and may be overturned in many locations (Fig. 2). Our observations are consistent with Vlasov et al. (1991) who mapped the main strand of the Darvaz Fault along the base of the Dashtijum Valley within upper Jurassic units, suggesting a bedding-parallel fault. The structural character and stratigraphic position of the Darvaz Fault suggests that it is an exposed part of the Jurassic décollement that underlies that rest of the TFTB (Fig. 3). Previous geologic (Trifonov, 1978) and geodetic (Mohadjer et al., 2010) studies have suggested the Darvaz Fault is an active sinistral strike-slip fault. However, evidence for strike-slip displacement across the Darvaz Fault zone in the Dashtijum Valley was not observed.

East of the Darvaz Fault, Permian carbonate rocks rest unconformably on Carboniferous and older metamorphic rocks (Fig. 2, 3). Thus, the Dashtijum Valley region represents a relatively complete stratigraphic section, from Paleozoic metamorphic basement in the Pamir to synorogenic Neogene sedimentary deposits in the Tajik Basin, with a bedding-parallel décollement (the Darvaz fault) in the Jurassic. There is no evidence that the Jurassic and younger stratigraphic section has been thrust more than a few km beneath the Pamir margin along the Darvaz Fault. Instead, the Mesozoic and younger section was uplifted above the Pamir margin, perhaps as a passive roof duplex (e.g., Banks and Warburton, 1986). This is a critical observation that suggests the Mesozoic and younger sedimentary rocks of the Tajik Basin were not subducted beneath the Pamir margin. Transfer of slip from deeper stratigraphic or crustal levels in the Pamir to the Jurassic décollement in the Tajik Basin must occur on structural ramps located deeper in the subsurface as shown in Figure 3, bypassing the Darvaz Fault. As a result, the amount of slip on the bedding-parallel Darvaz Fault in the Dashtijum region is likely small (< 10 km) and should be only a fraction of the total estimated shortening in the TFTB. The total estimated shortening in the East TFTB is ~30 km, which is unlikely to be a gross underestimate because all of the major structures have hangingwall cut-offs preserved along strike. Increasing the magnitude of slip on the Darvaz Fault requires reducing the amount of Tajik Basin lithosphere underthrust beneath the Pamir.

Other faults besides the main Darvaz Fault are present in the Dashtijum Valley, including an unnamed reverse fault dipping moderately to steeply eastward that places Permian carbonate rocks over overturned lower Jurassic clastic rocks (Fig. 2, 3). Based on reports of the thickness of the Jurassic and Permian sections in the Dashtijum Valley region (Leven et al., 1992), there is minimal stratigraphic separation across this fault and it cannot be a major thrust ramp. Vlasov et al., (1991) indicated local faulting along the Jurassic-Permian contact in the Dashtijum Valley region as well, but showed that these faults tip-out within 10 km along-strike and that the Jurassic-Permian contact is largely an unconformable (depositional) contact along the northwest margin of the Pamir (Fig. 2). Based on the limited along-strike extent and minimal stratigraphic separation, these faults at the Jurassic-Permian contact are not interpreted to have significant displacement or to be major, unrecognized strands of the Darvaz Fault.

A plausible fault is shown above the modern erosion level in the Dashtijum region that breaches the anticline-syncline pair. This fold pair is interpreted to have originated as a detachment fold that formed above the Jurassic decollement, similar to the Vakhsh fold and other folds in the East TFTB (Fig. 3A). The fault breaching the fold pair is not required to exist, but it may link with, or have been reactivated by, the fault that offsets the Jurassic-Permian contact. The reverse fault offsetting the Jurassic-Permian contact may have cut-up section and through the Jurassic decollement, offsetting the decollement and younger stratigraphic section (dashed fault in Fig. 3A). The high angle between this fault and the projection of the Jurassic decollement (Darvaz Fault) suggest it may have formed after the proposed passive roof duplex (Fig. 3).

Peter 1st Range and Northern Pamir

Cross-section B-B’ illustrates that the Peter 1st Range consists of a single large thrust sheet associated with the PFT (Fig. 3D). The leading edge of the PFT thrust sheet contains a tight, upright to overturned anticline-syncline pair that can be observed along much of the Vakhsh River. Folds in the

PFT thrust sheet are nearly similar (class II; Ramsey and Huber, 1987). Along strike to the southwest, the PFT splits into a series of thrust faults and folds that make up the East TFTB (Fig. 2). No Permian to Jurassic sedimentary rocks are present in the Tian Shan, but they are inferred to appear and thicken to the south and east. Two faults mark the position of the MPT in cross-section B-B', which are referred to here as the north MPT and south MPT (Fig. 2, 3D). In the plane of section, the north MPT places upper Cretaceous rocks on Miocene rocks with ~2 km of stratigraphic separation. However, within ~ 5 km along strike to the northeast, the stratigraphic separation on the north MPT decreases to zero or near zero (Fig. 2), indicating that the north MPT is both a hangingwall ramp and footwall ramp in the plane of section with limited (< 5 km) displacement (Fig. 3). The north MPT continues along strike to the northeast (near 71°E longitude), where Vlaslov et al. (1991) mapped the structure as a bedding-parallel fault that separates the lower Cretaceous and Jurassic sections. The north MPT here may be a thrust flat, whose slip is constrained by the thrust ramp along strike; alternatively, it may not be a fault contact. The lower Cretaceous-Jurassic contact was mapped by Vlaslov et al. (1991) as a depositional contact west of 71°E longitude (Fig. 2). The north MPT cross-cuts the Jurassic decollement and appears to have formed after slip on the PFT. Slip on the north MPT, post-dating and cross-cutting the Jurassic decollement, is similar to the fault that offsets the Permian-Jurassic contact in the Dashtijum Valley (Fig. 3A, dashed fault), which may also cross-cut Jurassic decollement at a high-angle, although direct evidence for this structural relationship has been eroded in the Dashtijum region.

The south MPT was mapped by Vlasov et al (1991) as a bedding-parallel fault separating the Jurassic and Permian sections with little to no stratigraphic separation. It is overlapped by Neogene synorogenic sedimentary rocks to the southwest along strike. Along strike to the northeast, the Jurassic-Permian contact is mapped as a depositional contact, similar to the Jurassic-Permian contact relation in much of the Dashtijum Valley region (Fig. 2). Where the south MPT cuts across stratigraphic section (east of 71°E longitude) it displays little to no stratigraphic offset, indicating minimal (< 2 km) displacement (Fig. 2). Like the north MPT, the south MPT may not be a fault, may only have localized slip, or could be a flexural-slip fault that accommodates differential movement of beds while folding.

The Northern Pamir is a broad anticlinorium that is defined by gently folded Permian volcaniclastic and sedimentary rocks deposited in angular unconformity on penetratively deformed Paleozoic meta-sedimentary rocks and Proterozoic (?) rocks (Fig. 2, 3). In addition to the Permian rocks, deformation structures in the Paleozoic section within the Northern Pamir are cross-cut by plutonic rocks, likely of Triassic age (Schwab et al., 2004); this suggests little to no late Mesozoic to Cenozoic internal deformation in the Northern Pamir, consistent with the observations of Burtman and Molnar (1993). The anticlinorium in Northern Pamir is interpreted to have been formed above a large basement ramp (Fig. 3D, cross-section B-B'). The contact relationships along the Pamir margin show that the Mesozoic to

Cenozoic sedimentary rocks in the Tajik Basin were deposited on top of the Northern Pamir and were subsequently eroded. The thickness and original extent into the Pamir of these deposits are unknown. The thin-skinned thrust structures in the TFTB and Peter 1st Range may have also been present above the Northern Pamir prior to uplift and erosion, which could help balance shortening in the Paleozoic section (Fig. 3). Cross-section B-B' suggests 55-60 km of total shortening, which is similar to previous estimates for the Peter 1st Range (Hamburger et al., 1992).

The Permian rocks in the Northern Pamir are truncated to the south by a steeply dipping shear zone that juxtaposes meta-sedimentary rocks against Permian rocks (Fig. 2, 3). The shear zone is referred to here as the Dashtak shear zone, which is the name of a small village near its exposure along the Panj River (Fig. 2). The metasedimentary rocks were originally mapped as Carboniferous (Vlaslov et al., 1991), but are here interpreted to be part of the Karakul-Mazar accretionary complex, which Robinson et al. (2012) showed to be Triassic in age in the Chinese Pamir. The suture zone between the Northern Pamir and Central Pamir terranes is the Tanymas Fault (Fig. 2). No attempt was made to incorporate deformation south of the Dashtak shear zone into cross-section B-B' (Fig. 3D), but a cross-section for this region is presented in Stearns et al. (2015).

Structure below the Jurassic Décollement

In both the East and West TFTB, in cross-section A-A', there is significant structural relief on the upper Jurassic décollement (Fig. 3A). The nature and timing of development of this relief are of particular interest because Middle Jurassic carbonate rocks, located below the décollement, are potential hydrocarbon reservoirs (Ulmishek, 2004). One possible explanation for the structural relief of the Jurassic décollement is lithospheric flexure in response to loading (Fig. 4). The Tajik Basin is an active flexural basin with thick accumulations of synorogenic deposits adjacent to the Tian Shan and Pamir. Iterative modeling suggests a flexural rigidity of 5×10^{22} Nm for the Tian Shan side of the basin and a flexural rigidity of 1×10^{22} Nm for the Pamir side of the basin (Fig. 4). The shallower décollement dip beneath the West TFTB suggests a higher flexural rigidity, which may reflect older lithospheric domains located farther away from the Pamir. This indicates that a reasonable range of flexural rigidities and loads can match the estimated geometry of the Jurassic décollement. The presence of two loads results in a composite flexural high separating the Tian Shan and Pamir flexural depocenters. A similar composite flexural response is found in the Adriatic Sea where the Puglia high separates the Apenninic and Hellenic foreland basins (Allen and Allen, 2013). The modeled flexural high is centered near the Yovon Valley. Although this composite flexural geometry can explain much of the structural relief on the Jurassic décollement (Fig. 4), additional shorter-wavelength structural relief on the décollement requires additional mechanisms other than flexure.

Previous interpretations of the TFTB have suggested that relief on the Jurassic décollement may largely be a result of thickening and movement of salt within the Guardak Formation (Bekker, 1996). Assuming sub-horizontal Paleozoic rocks beneath the décollement and no salt beneath the structurally lowest parts of the TFTB, area balancing suggests that an initial horizontal layer of salt >3 km thick is required to explain the structural relief. Exposures of the Guardak Formation in the southwest Gissar Mountains are 350 to 400 m thick (Mesezhnikov, 1988) and even the thickest parts of the Guardak Formation in the undeformed Amu Darya Basin to the west in Turkmenistan are < 1 km thick (Ulmishek, 2004). These observations suggest that thickening in response to salt movement alone could not have produced the relief on the Jurassic décollement.

Another possible explanation for the structural relief on the Jurassic décollement is deformation of Paleozoic and older basement rocks. Basement-involved structures are exposed on the margins of the Tajik Basin in both the Tian Shan and Pamir and the proposed basement geometry at depth in the Tajik Basin helps to balance shortening in the upper crust. Alternatively, shortening in the upper crust could be balanced by shortening of the basement entirely beneath/within the Pamir and Tian Shan. Earthquakes in the Tajik Basin indicate deformation at depths below the inferred position of the Jurassic décollement (Fan et al., 1994). Existing interpretations for basement deformation in the TFTB suggest that basement blocks are uplifted by high-angle reverse faults and that these faults may locally offset the Jurassic décollement (Thomas et al., 1994; Bourgeois et al., 1997). Apart from the mountain front faults bounding the Tajik Basin, there is no clear evidence that basement faults offset the Jurassic décollement. Here, we interpret the basement-involved faults to merge with the Jurassic décollement, which may act as a roof thrust to a large duplex in the Paleozoic and older section. The Jurassic décollement is folded above these basement structures and shortening occurred after or contemporaneous with the shortening recorded in the Cretaceous and younger stratigraphic section. It is likely that some combination of basement faulting and salt movement was superimposed upon a flexural signal to produce the modern structural relief on the Jurassic décollement. The timing and amount of slip on these faults is assessed below.

Low-Temperature Thermochronologic Data

Apatite (U-Th)/He and Apatite Fission Track Results

AHe ages are presented in Table 1 and data from AHe analyses of individual aliquots are presented in supporting information Table S2. AHe ages reported in Table 1 are weighted mean averages of individual aliquots. All of the AHe ages are significantly younger than the respective depositional age of the sedimentary rock hosting the apatites (Late Cretaceous) except for samples IS-13-06 and IS-13-07, which were collected from Neogene deposits within the Tajik Basin (Fig. 2, 3). AHe cooling ages in the Tajik Basin range from 12.4 ± 4.6 Ma to 1.2 Ma ± 0.4 Ma and show a general decrease in age towards the geographic center of the Tajik Basin, around Yovon Valley (Fig. 3). Samples that deviate from this pattern are IS-13-01 and IS-13-03 from the Bobotogh thrust sheet, sample 14-05 from the Sarsarak thrust sheet, and DS-13-08 and DS-13-01 from the Dashtijum Valley (Fig. 3). There are no discernable age-eU (effective Uranium content) trends in the data, except for samples DS-13-01 and DS-13-08, which have a positive age-eU trend and sample 14-08 that may have a slight negative age-eU trend, although the range of eU values is relatively restricted for this sample (supporting information Figure S2). Data from DS-13-01 and DS-13-03 were not used in subsequent thermokinematic modeling.

AFT central ages are presented in Table 1 and data for each AFT sample analysis are presented in supporting information Table S3. AFT cooling ages range from 16.7 ± 4.1 Ma to 3.6 ± 1.1 Ma and are all significantly younger than the Late Cretaceous age of the sandstone hosting the apatite grains. The AFT ages are all within 4 Myr of the AHe cooling age for the same sample, except for sample IS-13-03, for which the AFT age is significantly older (16.7 ± 4.1 Ma) than the AHe age (3.0 ± 1.0). Single-grain analyses of sample IS-13-03 show relatively little age dispersion (Table S3), which indicates that IS-13-03 may be fully reset after deposition. Apatite grains from sample SHSH-95 had very low uranium concentrations and many grains displayed no spontaneous tracks. The average AFT age for sample SHSH-95 from grains with spontaneous tracks is 5.8 Ma ± 1.5 Ma and the oldest single grain age is 6.8 ± 6.9 Ma. The AFT age for sample SHSH-95 is estimated to be < ca. 7 Ma, with no lower age constraint, except for the AHe age estimate of 5.1 ± 1.6 Ma for the same sample if we assume that there is no age inversion (AHe cooling ages > AFT cooling ages). Like the AHe data, AFT cooling ages decrease toward the center of the Tajik Basin and Yovon Valley (Fig. 3). Also like the AHe data, sample 14-05 from the Sarsarak thrust sheet deviates from this trend and yields younger AFT ages. All of the AFT data were used to constrain thermokinematic modeling.

Interpretation of AFT and AHe Results

Except for samples IS-13-06 and IS-13-07, which were collected from Neogene sandstone, all of the AHe and AFT ages are interpreted to be fully reset and thus record cooling and exhumation associated with thrust activity. The range of AHe ages in samples IS-13-06 and IS-13-07 can be considered detrital ages which suggests a Pliocene maximum depositional age. Individual aliquots from AHe samples show a range of ages, but there is no clear clustering of data or correlations between aliquot ages and eU, excluding samples DS-13-01 and DS-13-08 as discussed above. AHe sample ages in Table 1 are interpreted to represent a single age population and are weighted means of all aliquots reported in Table S2.

Thermokinematic Modeling

Thermokinematic modeling was only performed on cross-section A-A', for which thermochronologic data were obtained. Modeling consists of a baseline model (preferred model) in which the timing and magnitude of slip on the major faults/folds and the basal temperature were adjusted iteratively until an acceptable fit was achieved between the predicted thermochronologic cooling ages and the measured (observed) cooling ages and between the predicted model geothermal gradient and the modern geothermal gradient (Fig. 6, 7). Next, a suite of models were run to assess how changing the basal temperature or the timing of slip affects the results of the baseline model.

Baseline (preferred) Model

Figure 6 presents a preferred "baseline" model that returns predicted AHe and AFT ages from FETKin forward modeling that are in close agreement with the measured AHe and AFT ages. It should be emphasized that the results are non-unique and are not inverted to determine a "best-fit" model. The results are presented as a plausible scenario constrained by the available structural and thermochronologic data (e.g., Ballato et al., 2013). The basal temperature (at 25 km depth) that most closely reproduced the modern geothermal gradient was 500°C (Fig. 6). The magnitude and timing of slip on the major structures in the TFTB for the baseline model is presented in Table 2 and shown graphically in the incrementally restored cross-sections of Figure 5. The results suggest that deformation in the TFTB started at the margins of the Tajik Basin, adjacent to the southwest Gissar Range during the middle Miocene and adjacent to the Pamir Mountains during the late Miocene. Throughout the Miocene and into the Pliocene, deformation propagated towards the center of the Tajik Basin and Yovon Valley. Cumulative shortening within the confines of the model is ~60 km and indicates a middle Miocene to present shortening rate of ~4 to 6 mm/yr (Fig. 9). The Pliocene to present shortening rate is similar or slightly faster, ~ 6 to 8 mm/yr, which is consistent with estimates of modern shortening rates (5-10 mm/yr) calculated from GPS studies (Ischuk et al., 2013). Subsequent suites of models, presented below, were run to test the robustness of the shortening rate and its acceleration during the Pliocene.

There is a spatial correlation between the location of the highest structural relief on the Jurassic décollement and the youngest AHe and AFT cooling ages (Fig. 3, 6). Slip on the basement structures and folding of the Jurassic décollement are interpreted to be Pliocene in age, contemporaneous with or post-dating deformation on the major thrust faults and folds. Cooling through the retention/annealing zones was primarily related to faulting and folding above the Jurassic décollement and locally influenced by uplift on basement structures (Fig. 6).

Models that reproduce the small differences between the measured AHe and AFT cooling ages require relatively short periods of rapid exhumation so that the modeled samples pass quickly through the partial retention zone (AHe) and partial annealing zone (AFT) towards the erosion surface. In turn, this suggests rapid slip on the thrust faults. More protracted periods of slip produce a greater difference between the two thermochronometers (e.g., Lock and Willett, 2008). The large difference between the AHe and AFT age for sample IS-13-03 from the hangingwall of the Bobotogh thrust fault indicates a long period of minor displacement, or no slip, after initial movement during the early to middle Miocene and then a reactivation of the Bobotogh thrust fault during the Pliocene. All other fault displacements and folds in the TFTB can be adequately modeled as single pulses of deformation.

Effects of Varying Basal Temperature

To explore the effects of varying the amount of heat in the system, a suite of models were run in which the basal temperature (a fixed parameter) was changed from the baseline model. The results of these models were compared against the observed thermochronologic ages and the modern geothermal gradient (Fig. 6, 7). Increasing or decreasing the basal temperature by 25°C has relatively little effect on the modeled AFT and AHe ages, which fit the observed cooling ages within error. Increasing or decreasing the basal temperature by 25°C also yielded final model geothermal gradients that were largely within the estimated range of the modern geothermal gradient (Fig. 7). Decreasing the basal temperature by 50°C (to 450 °C) resulted in partially reset (too old) AFT model cooling ages for the Bobotogh thrust sheet, Karshi thrust sheet, Rangon thrust sheet, and Sangyak anticline (Fig. 6). The decreased basal temperature also produced model geothermal gradients almost entirely below the estimated range of the modern geothermal gradient (Fig. 7). Raising the basal temperature by 50°C (to 550 °C) has relatively little effect on the model. AFT and AHe ages, except for perhaps the synthetic AFT ages in the Bobotogh thrust sheet. The subdued effect of higher basal temperatures on modeled cooling ages is because most synthetic thermochronologic samples are well below their respective annealing/retention zone depths prior to exhumation. Only the Bobotogh thrust sheet, which is interpreted to be reactivated in the last 2 Ma, spent time within the AFT partial annealing zone as a result of previous (early Miocene) slip. The period of previous slip on the Bobotogh thrust could be pushed forward in time to match the model AFT ages without affecting the model AHe ages for the 550 °C model, although the final geothermal gradients from this model are almost all above the estimated modern geothermal gradient (Fig. 7). The results from the suite of models that varied basal temperature indicate that the amount of heat in the system has relatively little effect on the predicted model thermochronologic cooling ages for synthetic samples that exhume quickly. There is a minimum amount of heat in the system, corresponding to a basal temperature of ~450 °C (or 50 °C below the baseline model), below which synthetic samples do no become fully reset. Conversely, the maximum amount of heat in the system is only constrained by the estimated modern geothermal gradient.

Effects of Varying Timing of Slip

Unlike the amount of heat within the model, varying the timing of slip on the structures in the model has significant effects on the synthetic cooling ages (Fig. 6). Cooling age changes were investigated by shifting the initiation of slip on the major structures in the baseline (preferred) model either 2 Myr earlier (toward the past) or 2 Myr later (toward the present). 2 Myr is the time step between the partially restored sections input into FETKin. Earlier slip resulted in partially reset synthetic AFT ages for the Bobotogh thrust sheet, the Karshi thrust sheet, and the Sangyak anticline and poor fits (outside of measured cooling age errors) for synthetic AFT and AHe ages for the Bobotogh, Aruntau, Jetimtau, and Karatau thrust sheets (Fig. 6). Delaying the initiation of slip on these faults/folds allows time for thicker accumulations of sediment as a result of flexural subsidence and can fully reset the synthetic AFT samples. However, because the observed AHe and AFT ages are relatively close together, exhumation must occur as a short-lived pulse of deformation. Synthetic AFT and AHe cooling ages for the model with later slip was within, or close to within, error for most of the measured thermochronoligical samples except for the samples from the Bobotogh thrust sheet, Aruntau thrust sheet, and Sangyak anticline (Fig. 6). The similarity between the late and early synthetic cooling ages for the Sarsaryak thrust sheet and Vakhsh anticline suggest that their exhumation may be largely controlled by uplift associated with slip on the faults in the Permian-Paleozoic section beneath the Jurassic décollement.

For all thrust sheets or folds for which the early model or late model synthetic cooling ages fell within error of the measured ages, the cumulative displacement is plotted and compared to the baseline model as a qualitative measure of uncertainty (Fig. 9). The results suggest that the mid-Miocene to present shortening rate is on the order of 4 to 6 mm/yr, while the Pliocene to present shortening rate is on the order of 6 to 8 mm/yr. The results cannot distinguish between a constant shortening rate (of ~ 6 mm/yr) from the Miocene to present and an acceleration of shortening in the Pliocene.

DISCUSSION

Structural Evolution of the Tajik Fold and Thrust Belt

Previous studies have suggested that uplift of the Pamir and central Tian Shan started in late Eocene to early Miocene (Sobel and Dumitru, 1997; Sobel et al., 2006; Heermance et al., 2008; DeGrave et al., 2012; Sobel et al., 2013; Smit et al., 2014; Carrapa et al., 2015). Unpublished AHe and AFT from the southwest Gissar Range also suggest that uplift may have started during the Miocene (Gagala et al., 2014). The results show that deformation migrated out of the Tian Shan and Pamir and into the Tajik Basin during the middle Miocene to form the TFTB. In general, shortening in the TFTB is clustered near the center of the Tajik Basin (Fig. 3). Rapid synorogenic sedimentation in the Tian Shan and Pamir flexural basins may have suppressed deformation in these depocenters and shifted the locus of shortening toward the foreland (e.g., Stockmal et al., 2007; Fillon et al., 2013).

Deformation within the Tajik Basin began at the outer margins of the TFTB and propagated toward the center of the thrust belt (Fig. 3, 5, 6). Initial, contemporaneous shortening on faults and folds both proximal and distal to the hinterland (Pamir Mountains or southwest Gissar Range) prior to the establishment of a regional orogenic taper is inconsistent with most models for thrust belt mechanics on a single thrust wedge. Thrust wedges can exist in three states: subcritical, critical, and supercritical (Davis et al., 1983; Dahlen, 1984). Feedback loops in thrust belt systems tend to push thrust wedges toward a critical state with temporally restricted excursions into subcritical and supercritical fields (e.g., DeCelles and Mitra, 1995). In subcritical wedges, shortening is concentrated in the interior, proximal (toward the hinterland) parts of the thrust belt with no deformation at the foreland (distal) side. In critical wedges, deformation propagates uniformly into the foreland on more or less evenly spaced (self-similar) thrust sheets. In supercritical wedges, deformation is concentrated at the most distal structure and the entire thrust wedge in transported as a coherent wedge. The unique geometry and deformation history of the TFTB does not fit any of these descriptions and is better understood as two separate (critical) thrust belt wedges that have encroached upon one another. In this context, the peculiar inward vergence of the TFTB belt can be explained as a Tian Shan thrust belt verging toward the east and a Pamir thrust belt verging toward the west. None of the major thrust faults in the Tajik Basin is interpreted as a backthrust; instead, all of the major thrusts in the TFTB are foreland-verging thrust faults. The Yovon Valley, at the center of the TFTB, is the remnant of a shared foreland basin. The overall pattern of decreasing AHe and AFT cooling ages towards the center of the TFTB (Figs. 3, 5, 6) is a result of in-sequence propagation of deformation in both thrust belts, which is corroborated by structural observations such as progressive hindward steepening of thrust faults. In the two instances where cooling ages do not appear to decrease toward the center of the TFTB (the Bobotogh and Sarsarak thrusts), field relationships and thermokinematic modeling demonstrate that these represent reactivated or out-of-sequence faults.

Our interpretation suggests that the West TFTB is a thin-skinned thrust belt in the larger Tian Shan orogenic belt. The West TFTB records 35-40 km of shortening, which is similar to the amount of shortening (10-40 km) reported for thin-skinned fold-thrust belts all along the southern margin of the Tian Shan, including the Kashi, Kepingtage, and Kuqa segments (Yin et al., 1998; Heermance et al., 2008; Fu et al., 2010) (Fig. 1). In addition to similar magnitudes of shortening, the timing for deformation is comparable between the West TFTB and the central Tian Shan thrust belts. Uplift and exhumation of the central Tian Shan hinterland began during the late Oligocene to early Miocene and thin-skinned deformation migrated into the foreland in middle to late Miocene time (Sobel and Dumitru, 1997; Chen et al., 2007). Finally, shortening rates may have accelerated in both the West TFTB and the central Tian

Shan thrust belts during the Pliocene (Yin et al., 1998; Allen et al., 1999; Heermance et al., 2008), although the magnitude and effect of climate on this signal remains uncertain (Molnar, 2004). For example an increase in erosion within the Pamir as suggested by a global acceleration in mountain erosion during the Pliocene (Hermann et al., 2013) would predict the wedge to deform internally to adjust for taper, rather than having deformation migrate outward into the foreland as observed in the TFTB. The similarity in structural character, magnitude of shortening, and timing of deformation for > 1,000 km along strike of the southern margin of the Tian Shan are representative of a kinematically linked orogenic system (Fig. 1). Stress from the India-Asia collision is transferred through the old and strong Tarim-Tajik lithosphere to the relatively young and weak lithosphere that forms the Tian Shan (Molnar and Tapponnier, 1975; 1981; Tapponnier and Molnar, 1979; Avouac et al., 1993), which explains the broad synchroneity of deformation throughout the Tian Shan.

The structural configuration at different locations along the Tian Shan orogenic system may provide a template for understanding how systems like the TFTB have evolved. Figure 10 shows schematic cross-sections across the Tarim Basin, Tajik Basin, and Alai Valley that all show oppositely verging thrust belts. The differences between cross-sections are primarily related to the distance between the Tian Shan and Pamir/Tibetan orogens. With continued shortening, the structural style of the TFTB may resemble the Alai Valley with overlapping thrust systems, as suggested by Pavlis et al. (1997) for the Peter the First Range and Alai Valley regions.

Origin of the Northern Pamir

Along the boundary between the Pamir and the Tajik Basin the upper Jurassic to Cenozoic sedimentary rocks of the Tajik Basin are either in depositional contact with lower Jurassic to Paleozoic rocks or are separated from these rocks by a bedding-parallel fault. Only locally do strands of the MPT or Darvaz Fault have contact relationships indicative of thrust ramps, and when they do, the stratigraphic separation across these ramps suggests limited displacement (< 5 km). We propose that in many locations, the Darvaz Fault-MPT system is a bedding-parallel décollement that was folded and uplifted along with the stratigraphic section. For example, the bedding-parallel Darvaz fault in the Dashtijum Valley region is interpreted to be an exposure of the Jurassic décollement present throughout the TFTB (Fig. 3A). Structural reconstructions suggest that the sedimentary rocks of the Tajik Basin were deposited on the Northern Pamir and subsequently uplifted and eroded. The structural geometry of the northwest Pamir margin can be characterized as a frontal monocline (Couzens-Schultz et al., 2003), similar to the Sulaiman Range in Pakistan (Banks and Wharburton, 1986) and the frontal Alberta thrust belt of western Canada (Price, 1986; Vann et al., 1986). These types of structures have also been described as mountain front flexures or basement steps where a large thrust ramp exhumes deeper structural levels and uplifts the overlying sedimentary cover (McQuarrie, 2004). Deformation style commonly transitions from thick-skinned to thin-skinned across these boundaries (e.g., Bolivian Andes; Kley, 1996). Unlike the Central and Southern Pamir terranes, the Northern Pamir has been part of Asia since at least the Late Carboniferous, perhaps longer (Burtman and Molnar, 1993). We propose that the Northern Pamir is simply the uplifted and deformed edge of the Tajik lithosphere. This interpretation requires that the Tajik Basin crust was incorporated into the Pamir during orogenic growth, rather than subducted beneath the Pamir.

Implications of Shortening Estimates

Geological and geophysical evidence indicates that shortening in the central Tian Shan thrust belts (10-40 km) is a result of underthrusting of the Tarim lithosphere (Abdrakhmatov et al., 1996; Allen et al., 1999; Sobel et al., 2006; Li et al., 2009; Lei et al., 2011; Gao et al., 2013; Gilligan et al., 2014). Thrust faults in the West TFTB are kinematically linked to the expansion of the Tian Shan and shortening in the West TFTB is similarly related to underthrusting of the Tajik Basin lithosphere beneath the southwest Gissar Range. This distinction is important because shortening in the West TFTB should not be used to balance potential subduction of Tajik-Tarim lithosphere beneath the Pamir (Burtman and Molnar, 1993).

In addition to shortening in the West TFTB, our results indicate 20-25 km of basement-involved shortening within the southwest Gissar Range that is related to the growth of the Tian Shan. Previous estimates of shortening across the TFTB have included deformation within the southwest Gissar Range (Thomas et al., 1994; 1996; Bourgeois et al., 1997), but like the West TFTB this shortening should not be included in estimates for the length of lithosphere underthrust beneath the Pamir. Discarding shortening in the West TFTB and southwest Gissar Range leaves only ~30 km of shortening in the East TFTB that could be attributed to intracontinental subduction beneath the Pamir (Burtman and Molnar, 1993). This amount of shortening is comparable to estimates of shortening in the Peter the First Range (< 60 km) (Leith and Alvarez, 1985; Hamburger et al., 1992; Bekker, 1996), the Alai valley (< 20 km) (Coutand et al., 2002), and on the northeast margin of the Pamir (30-35 km) (Li et al., 2012). These results are an order of magnitude less than the 250-300 km length of Tajik-Tarim lithosphere proposed to have subducted beneath the Pamir Mountains (Burtman and Molnar, 1993). Although the exposure of hangingwall cut-offs in the East TFTB suggests that the estimate of shortening is not grossly underestimated, the restored cross-section A-A' (Fig. 3B) does represent conservative (minimum) values. However, even if the estimated amount of shortening in the East TFTB was doubled or tripled (for which there is no evidence) or if the amount of shortening in the West TFTB was included, there is still not enough shortening to balance the 250-300 km length of the "Pamir slab."

In order to reconcile models of intracontinental subduction with the lack of evidence for shortening in the upper crust, some authors have proposed that upper to middle crustal rocks were subducted beneath the Pamir and then underplated, interleaved into the Pamir crust, or subducted along with the lower crust and mantle lithosphere (Burtman and Molnar, 1993; Mechie et al., 2012; Schneider et al., 2013; Sippl et al., 2013; Sobel et al., 2013). By subducting or underplating the upper crust, the record of shortening may be destroyed and any correlation between the magnitudes of shortening and subduction may not be necessary. However, the results of this study suggest that the rocks in the eastern part of the Tajik Basin were neither underthrusted nor subducted, but were uplifted and eroded above the Pamir or incorporated into the upper structural levels of the Pamir. A relatively complete stratigraphic section of metamorphic Paleozoic basement rocks through Neogene synorogenic rocks is exposed all along the northwest margin of the Pamir. This observation links together the Tajik Basin and Northern Pamir and eliminates the possibility of significant subduction of the Tajik Basin lithosphere beneath the Pamir.

If intracontinental subduction of Asian lithosphere is not occurring beneath the Pamir, what is generating earthquakes in a contorted Benioff zone and what could be producing the low-velocity zone at such great depths in the mantle (Roecker, 1982; Koulakov and Sobolev, 2006; Schneider et al., 2013; Sippl et al., 2013)? We suggest that the lowermost crust and mantle lithosphere of the Pamir have delaminated or foundered into the mantle (Fig. 11). The delaminated lithosphere in the upper mantle beneath the Pamir is part of the Northern, Central, and Southern Pamir terranes, rather than cratonic Asian lithosphere (e.g., Kufner et al., 2016; Rutte et al., 2017b). In this model, there is no requirement for shortening of the Asian lithosphere in the Pamir foreland and the kinematics of the TFTB, including the MPT, may be partially or wholly unrelated to the delaminated material. Likewise, the timing and rate of delamination are not necessarily related to the rate or amount of shortening at the Pamir margin.

Fast seismic velocities beneath the Pamir crust suggest that Indian mantle lithosphere extends as far north as the Central Pamir terrane (Mechie et al., 2012; Sippl et al., 2013). Thus, a first-order observation is that the original mantle lithosphere beneath the Pamir is missing and has been replaced by Indian mantle lithosphere. India has been subducting continuously beneath the Pamir since at least ~20-25 Ma, when many researchers have proposed a slab break-off event or roll-back of the Indian continental lithosphere (Mahéo et al., 2002; Replumaz et al., 2010; Amidon and Hynek, 2010; DeCelles et al., 2011; Carrapa et al., 2014). Since that time, India and Asia have been converging at a roughly steady rate of ~4-5 cm/yr (DeMets et al., 1990; Bilham et al., 1997; Molnar and Stock, 2009). Assuming that all of this convergence was accommodated in the Indian mantle lithosphere by underthrusting beneath the Pamir, as suggested by Negredo et al. (2007), it is possible to restore the leading edge of Indian mantle lithosphere 100-125 km to the south, near the Karakoram batholith (Fig. 11). The resulting gap in mantle lithosphere beneath the Pamir is roughly equivalent to the along-arc length of the Pamir seismic zone, which can be "restored" to fit beneath the Pamir (Fig. 11). Indentation of India may be actively facilitating northward delamination of mantle lithosphere (Stearns et al., 2015; Kufner et al., 2016; Rutte et al., 2017b), analogous to the model for the removal of Qiantang mantle lithosphere in Tibet during the Eocene (DeCelles et al., 2011). The Qiantang terrane and the Southern/Central Pamir terranes are equivalent along strike of the orogen (Robinson et al., 2012). The exact mechanisms for this lithospheric interaction at depth are unclear, but Stearns et al. (2015) suggested the increased gravitational potential energy ± mantle downwelling could have triggered delamination/roll-back. If the start of delamination is related to the resumption of Indian underthrusting following the late Oligocene to early Miocene slab-breakoff event, it would indicate delamination also started at that time. A possible argument against the initiation of delamination during the early Miocene is that the delaminated material may have sunk deeper into the upper mantle than is currently imaged today. The depth of the Pamir slab indicates a sinking velocity on the order of 10 mm/yr, assuming early Miocene delamination. Sinking velocities can be approximated using a Stokes sinking sphere (Morgan, 1965). A sinking velocity of ~10 mm/yr is consistent with a sphere with radius of 55 km and 50 kg/m^3 excess density in an upper mantle with constant viscosity of 10^{21} Pa·s. This back-of-the-envelope sinking velocity estimate is poorly constrained, but it does suggest that a 10 mm/yr velocity is within the realm of feasibility. Alternate hypotheses suggest that roll-back or delamination of the Pamir slab started in the late Miocene (Kufner et al., 2016; Rutte et al., 2017b).

Roll-back of subducted Asian lithosphere has been suggested to have caused a change in boundary forces in the upper plate (Pamir orogen) that could drive extension within the Pamir and may explain the initiation of extension in the Pamir gneiss domes at ~ 20 Ma (Sobel et al., 2013; Stearns et al., 2015). An alternative explanation for initiation of gneiss dome extension is the delamination of (potentially eclogitized) Pamir lower crust and mantle lithosphere, which would regionally raise gravitational potential energy and would not require a change in boundary forces (e.g., Molnar and Lyon-Caen, 1988). Delamination was originally envisioned as a peeling away of the mantle lithosphere along the Moho (Bird, 1979); however, recent studies have shown that delamination may occur within the lower crust in response to eclogitization (Sobolev et al., 2006; Krystopowicz and Currie, 2013; Currie et al., 2015). The timing of crustal thickening in the Pamir is unclear (Robinson, 2015), but most researchers suggest that it occurred from the late Eocene to early Miocene based on prograde metamorphic ages measured in the Pamir gneiss domes (Schmidt et al., 2011; Stearns et al., 2013). On the other hand, Smit et al. (2014) suggested that prograde metamorphism may be related to high mantle heat flow following detachment of the Tethyan oceanic lithosphere during the Eocene. The Smit et al. (2014) model favors earlier (Cretaceous) Cordilleran-style crustal thickening in the Pamir as proposed by Robinson et al. (2012). In either model, crustal thickening in the Pamir may have been sufficient to eclogitize the lower crust. Evidence for eclogitization comes from eclogitic xenoliths in the Southern Pamir terrane, which were derived from Pamir crust and were buried to depths >90 km prior to magmatic entrainment and surface eruption during the middle to late Miocene (Ducea et al., 2003; Hacker et al., 2005; Gordon et al., 2012). Foundering or delamination of lower Pamir crust along with mantle lithosphere is one possible mechanism to generate these xenoliths (Gordon et al., 2012). Thus, the low-velocity zone beneath the Pamir (e.g., Sippl et al., 2013) may represent delaminated lower crust, rather than subducted lower crust of the Tajik-Tarim (Asian) lithosphere (Fig. 11). Foundering of the lithosphere beneath the Pamir may also explain the seismic gap (Peglar and Das, 1998) located between a cloud of deep mantle seismicity and shallow crustal seismicity associated with ongoing shortening at the northern margin of the Pamir (Fig. 11) (Schurr et al., 2014). The deficit of shortening in the Pamir and TFTB leaves open an important question: how did the Pamir crust thicken? If internal shortening and intracontinental subduction are not responsible for the thick crust in the Pamir, then upper crustal shortening in the Himalaya and northward underthrusting of Indian lithosphere remain a viable mechanism (Kapp and Guynn, 2004).

CONCLUSIONS

New AHe and AFT thermochronologic data indicate that deformation in the thin-skinned TFTB initiated during the middle Miocene. Sequential reconstructions of a balanced cross-section (Fig. 3) and thermokinematic modeling (Fig. 6, Table 2) suggest ~70 km of total shortening in the TFTB with a Miocene to present shortening rate of 4-6 mm/yr and a Pliocene to recent shortening rate of 6-8 mm/yr. Deformation in the TFTB propagated toward the center of the Tajik Basin, migrating away from both the southwest Gissar Range and the Pamir almost simultaneously. The West TFTB and East TFTB are two distinct thrust belts that have propagated toward each other (Fig. 3, 5, 6). Field observations and modeling results indicate that these two thrust belts generally display in-sequence patterns for fold and thrust propagation. The East TFTB has propagated from the Pamir and the West TFTB has propagated from the southwest Gissar Range of the Tian Shan. The structural style, timing of deformation, and magnitude of shortening in the West TFTB are consistent with thin-skinned thrust belts located along the northwest margin of the Tarim Basin. The West TFTB is part of the greater Tian Shan orogenic system and is related to northwestward underthrusting of the Tajik-Tarim lithosphere. As a result, as little as 30 km of shortening recorded in the TFTB is related to underthrusting of the Tajik lithosphere beneath the Pamir. This amount of shortening is not consistent with models that propose ~300 km of subducted continental lithosphere to explain deep seismicity and fast seismic velocities beneath the Pamir (e.g., Burtman and Molnar, 1993).

In addition to this shortening deficit, the structural architecture of the northern Pamir margin is consistent with a convergent orogenic margin rather than a subduction zone. A 10-15 km crustal section, spanning Paleozoic metamorphic basement to Neogene synorogenic sedimentary rocks, is exposed in a large frontal monocline along the northern margin of the Pamir. The Northern Pamir and Tajik Basin are part of the same lithospheric assemblage that has been incorporated into the Pamir during orogenesis. Mesozoic sedimentary rocks, and perhaps thin-skinned structures, like those observed in the TFTB, were once present above the Northern Pamir before being uplifted and eroded. There is no evidence for underplating or interleaving of upper to middle crust.

The ~300 km long, south-dipping zone of deep seismicity beneath the Pamir (e.g., Schneider et al., 2013) is not related to subduction of Asian lithosphere, but may be associated with the delamination of Pamir lower crust and mantle lithosphere (Fig. 11). This delamination may be facilitated by subducted Indian mantle lithosphere (Kufner et al., 2016; Rutte et al., 2017b). Although the geometry of the proposed delaminated lithosphere is similar to that shown in models that propose roll-back of subducted Asian lithosphere (Sobel et al., 2013; Stearns et al., 2015), these two models have distinct mechanical and geodynamic implications. Subduction roll-back is fundamentally driven by lower plate processes, primarily slab buoyancy and rate of subduction (Schellart, 2008). In the case of the Pamir, removal of the middle to upper crust, by underthrusting, is required to raise the integrated density of the lithosphere and allow continental subduction to be self-sustaining (Molnar and Gray 1979; Burtman and Molnar, 1993). This model predicts that slab forces would be driving upper plate shortening, recorded by deformation along the MPT, analogous to a subduction accretionary complex (e.g., Sobel et al., 2013). Conversely, delamination of continental mantle lithosphere is fundamentally controlled by upper plate processes, primarily crustal thickening or magmatic emplacement (Bird, 1979; Ducea and Saleeby, 1998). In the case of the Pamir, orogenic thickening, perhaps starting as early as the Cretaceous (Robinson, 2015) may have primed the lithosphere for delamination by moderately thickening the crust prior to India-Asia collision. Shortening recorded on the MPT and in the TFTB may be largely decoupled from the foundering lithosphere. Increased gravitational potential energy following lithospheric delamination is a plausible alternative to changes in boundary forces driven by slab migration to explain the initiation of Miocene extension as recorded in the Pamir gneiss domes.

Whereas delamination of continental mantle lithosphere is commonly observed in orogenic systems that have experienced protracted crustal thickening and/or concentrated arc magmatism (DeCelles et al., 2009; 2015; Wells et al., 2012; Beck et al., 2015), intracontinental subduction is a relatively rare phenomenon, for which the Pamir is the archetype (Burtman and Molnar, 1993). If intracontinental subduction is not occurring in the Pamir, as we propose, then it may be time to reevaluate whether it is a viable tectonic process at all and whether continental lithosphere can initiate and sustain subduction without the assistance of negatively buoyant oceanic lithosphere (e.g., Capitanio et al., 2010). Discriminating between crustal shortening and subduction in the interior of continental plates is critical for understanding the geodynamics of convergent orogenesis.

ACKNOWLEDGEMENTS

Research was supported by grants from the American Philosophical Society (JC), the American Association of Petroleum Geologists (JC), the Geological Society of America (JC), and Exxon Mobil Corporation (BC). Midland Valley provided MOVE software, TGS-NOPEC provided well log data, and LMKR provided GeoGraphix software. We thank Ecopetrol for use and development support of FETKin. Negmat Rajabov and Umed Sharifov aided in field and logistical support in Tajikistan. Discussions with Jerry Kendall and constructive reviews from Nadine McQuarrie and Michael Stearns significantly improved the quality of the manuscript.

REFERENCES CITED

Abdrakhmatov, K.Y., Aldazhanov, S.A., Hager, B.H., Hamburger, M.W., Herring, T.A., Kalabaev, K.B., and Zubovich, A.V., 1996, Relatively recent construction of the Tien Shan inferred from GPS measurements of present-day crustal deformation rates: Nature, v. 384, p. 450-453.

Allen, M.B., Vincent, S.J., and Wheeler, P.J., 1999, Late Cenozoic tectonics of the Kepingtage thrust zone: interactions of the Tien Shan and Tarim Basin, northwest China: Tectonics, v. 18, p. 639-654.

Allen, P.A., and Allen, J.R., 2013, Basin analysis: Principles and application to petroleum play assessment, Wiley-Blackwell, 642p.

Almendral, A., Robles, W., Parra, M., Mora, A., Ketcham, R.A., and Raghib, M., 2015, FetKin: Coupling kinematic restorations and temperature to predict thrusting, exhumation histories, and thermochronometric ages: American Association of Petroleum Geologists Bulletin, v. 99, p. 1557-1573.

Amidon, W.H., and Hynek, S.A., 2010, Exhumational history of the north central Pamir: Tectonics, v. 29, TC5017.

Angiolini, L., Zanchi, A., Zanchetta, S., Nicora, A., and Vezzoli, G., 2013, The Cimmerian geopuzzle: new data from South Pamir: Terra Nova, v. 25, p. 352-360.

Avouac, J.P., Tapponnier, P., Bai, M., You, H., and Wang, G., 1993, Active thrusting and folding along the northern Tien Shan and late Cenozoic rotation of the Tarim relative Dzungaria and Kazakhstan: Journal of Geophysical Research, v. 98, p. 6755–6804.

Ballato, P., Stockli, D.F., Ghassemi, M.R., Landgraf, A., Strecker, M.R., Hassanzadeh, J., Friedrich, A. and Tabatabaei, S.H., 2013, Accommodation of transpressional strain in the Arabia-Eurasia collision zone: new constraints from (U-Th)/He thermochronology in the Alborz mountains, north Iran: Tectonics, v. 32, p. 1-18.

Bally, A.W., Gordy, P.L., and Stewart, G.A,. 1966, Structure, seismic data, and orogenic evolution of southern Canadian Rocky Mountains: Bulletin of Canadian Petroleum Geology, v. 14, p. 337-381.

Banks, C.J., and Warburton, J., 1986, Passive-roof'duplex geometry in the frontal structures of the Kirthar and Sulaiman mountain belts, Pakistan: Journal of Structural Geology, v. 8, p. 229-237.

Bazhenov, M.L., and Burtman, V.S., 1986, Tectonics and paleomagnetism of structural arcs of the Pamir–Punjab syntaxis: Journal of Geodynamics, v. 5, p. 383–396.

Beck, S.L., Zandt, G., Ward, K.M., and Scire, A., 2015, Multiple styles and scales of lithospheric foundering beneath the Puna Plateau, central Andes, *in* DeCelles, P.G., Ducea, M.N., Carrapa, B., and Kapp, P.A., eds., Geodynamics of a Cordilleran Orogenic System: The Central Andes of Argentina and Northern Chile: GeologicalThe Geological Society of America Memoir 212, p.

Bekker, Y.A., 1996, Tectonics of the Afghan–Tadshik Depression: Geotektonika, v. 30, p. 76–82.

Bilham, R., Larson, K., and Freymueller, J., 1997, GPS measurements of present-day convergence across the Nepal Himalaya: Nature, v. 386, p. 61–64.

Bird, P., 1979,Continental delamination and the Colorado Plateau: Journal of Geophysical Research, v. 84, p. 7561–7571.

Bonini, M., 2007, Deformation patterns and structural vergence in brittle–ductile thrust wedges: an additional analogue modelling perspective: Journal of Structural Geology, v. 29, p. 141-158.

Bosboom, R., Dupont-Nivet, G., Huang, W., Yang, W. and Guo, Z., 2014, Oligocene clockwise rotations along the eastern Pamir: Tectonic and paleogeographic implications: Tectonics, v. 33, p. 53-66.

Bourgeois, O., Cobbold, P.R., Rouby, D., Thomas, J.-C., Shein, V., Shein, V., 1997, Least squares restoration of Tertiary thrust sheets in map view, Tajik Depression, Central Asia: Journal of Geophysical Research, v. 102, p. 27,553-27,573.

Boyer, S.E., and Elliott, D., 1982, Thrust systems: American Association of Petroleum Geologists Bulletin, v. 66, p. 1196-1230.

Brady, R.J., Ducea, M.N., Kidder, S.B. and Saleeby, J.B., 2006, The distribution of radiogenic heat production as a function of depth in the Sierra Nevada Batholith, California: Lithos, v. 86, p. 229-244.
Brookfield, M., and Hashmat, A., 2001, The geology and petroleum potential of the North Afghan platform and adjacent areas (northern Afghanistan, with parts of southern Turkmenistan, Uzbekistan and Tajikistan): Earth Science Reviews v. 55, p. 41–71.
Bullard, E.C., 1947, The time necessary for a bore hole to attain temperature equilibrium: Geophysical Journal International, v. 5, p. 127-130.
Burg, J.P., 2011, The Asia–Kohistan–India collision: review and discussion, *in* Brown, D., and Ryan, P., D., eds., Arc-Continent Collision: Springer, Berlin Heidelberg, p. 279-309.
Burtman, V.S., 2000, Cenozoic crustal shortening between the Pamir and Tien Shan and a reconstruction of the Pamir-Tien Shan transition zone for the Cretaceous and Palaeogene: Tectonophysics, v. 319, p. 69–92.
Burtman, V.S., and Molnar, P., 1993, Geological and geophysical evidence for deep subduction beneath the Pamir: Geological Society of America Special Paper, v. 281, 76p.
Capitanio, F.A., Morra, G., Goes, S., Weinberg, R.F. and Moresi, L., 2010, India–Asia convergence driven by the subduction of the Greater Indian continent: Nature Geoscience, v. 3, p. 136-139.
Carrapa, B., DeCelles, P.G., Wang, X., Clementz, M.T., Mancin, N., Stoica, M., Kraatz, B., Meng, J., Abdulov, S. and Chen, F., 2015, Tectono-climatic implications of Eocene Paratethys regression in the Tajik basin of central Asia: Earth and Planetary Science Letters, v. 424, p.168-178.
Carrapa, B., Mustapha, F.S., Cosca, M., Gehrels, G., Schoenbohm, L.M., Sobel, E.R., DeCelles, P.G., Russell, J. and Goodman, P., 2014, Multisystem dating of modern river detritus from Tajikistan and China: Implications for crustal evolution and exhumation of the Pamir: Lithosphere, v. 6, p. 443-455.
Carrapa, B., Trimble, J.D., and Stockli, D.F., 2011, Patterns and timing of exhumation and deformation in the Eastern Cordillera of NW Argentina revealed by (U-Th)/He thermochronology: Tectonics, v. 30.
Chen, J., Heermance, R., Burbank, D. W., Scharer, K. M., Miao, J., and Wang, C., 2007, Quantification of growth and lateral propagation of the Kashi anticline, southwest Chinese Tian Shan: Journal of Geophysical Research, Solid Earth, v. 112 (B3).
Coutand, I., Strecker, M.R., Arrowsmith, J.R., Hilley, G., Thiede, R.C., Korjenkov, A. and Omuraliev, M., 2002, Late Cenozoic tectonic development of the intramontane Alai Valley,(Pamir-Tien Shan region, central Asia): An example of intracontinental deformation due to the Indo-Eurasia collision: Tectonics, v. 21.
Couzens-Schultz, B.A., Vendeville, B.C., and Wiltschko, D.V., 2003, Duplex style and triangle zone formation: insights from physical modeling: Journal of Structural Geology, v. 25, p. 1,623-1,644.
Currie, C.A., Ducea, M.N., DeCelles, P.G., and Beaumont, C., 2015, Geodynamic models of Cordilleran orogens: Gravitational instability of magmatic arc roots: Geological Society of America Memoirs, v. 212, 22p.
Dahlen, F.A., 1984, Noncohesive critical Coulomb wedges: An exact solution: Journal of Geophysical Research: Solid Earth, v. 89, p. 10125-10133.
Dahlstrom, C.D.A., 1969, Balanced cross sections: Canadian Journal of Earth Sciences, v. 6, p. 743-757.
Davis, D., Suppe, J., and Dahlen, F.A., 1983, Mechanics of fold-and-thrust belts and accretionary wedges: Journal of Geophysical Research, v. 88, p. 1,153-1,172.
De Grave, J., Glorie, S., Ryabinin, A., Zhimulev, F., Buslov, M.M., Izmer, A., Elburg, M. and Vanhaecke, F., 2012, Late Palaeozoic and Meso-Cenozoic tectonic evolution of the southern Kyrgyz Tien Shan: Constraints from multi-method thermochronology in the Trans-Alai, Turkestan-Alai segment and the southeastern Ferghana Basin: Journal of Asian Earth Sciences, v. 44, p.149-168.

DeCelles, P.G. and Mitra, G., 1995, History of the Sevier orogenic wedge in terms of critical taper models, northeast Utah and southwest Wyoming: Geological Society of America Bulletin, v. 107, p. 454-462.
DeCelles, P.G., Ducea, M.N., Kapp, P., and Zandt, G., 2009, Cyclicity in Cordilleran orogenic systems: Nature Geoscience, v. 2, p. 251-257.
DeCelles, P.G., Kapp, P., Quade, J., and Gehrels, G.E., 2011, Oligocene–Miocene Kailas basin, southwestern Tibet: Record of postcollisional upper-plate extension in the Indus-Yarlung suture zone: Geological Society of America Bulletin, v, 123, p. 1,337-1,362.
DeCelles, P.G., Zandt, G., Beck, S.L., Currie, C.A., Ducea, M.N., Kapp, P., Gehrels, G.E., Carrapa, B., Quade, J. and Schoenbohm, L.M., 2015, Cyclical orogenic processes in the Cenozoic central Andes: Geological Society of America Memoirs, v. 212, p. 212-222.
DeMets, C., Gordon, R.G., Argus, D.F., Stein, S., 1990, Current plate motions: Geophysical Journal International, v. 101, p. 425–478.
DiPietro, J.A., and Pogue, K.R., 2004, Tectonostratigraphic subdivisions of the Himalaya: A view from the west: Tectonics, v. 23.
Donelick, R.A., Ketcham, R.A., and Carlson, W.D., 1999, Variability of apatite fission-track annealing kinetics: II. Crystallographic orientation effects: American Mineralogist, v. 84, p. 1,224-1,234.
Donelick, R.A., O'Sullivan, P.B., and Ketcham, R.A., 2005, Apatite fission track analysis: Reviews in Mineralogy and Geochemistry, v. 58, p. 49–94.
Ducea, M. and Saleeby, J., 1998, A case for delamination of the deep batholithic crust beneath the Sierra Nevada, California: International Geology Review, v. 40, p. 78-93.
Ducea, M.N., Lutkov, V., Minaev, V.T., Hacker, B., Ratschbacher, L., Luffi, P., Schwab, M., Gehrels, G.E., McWilliams, M., Vervoort, J. and Metcalf, J., 2003, Building the Pamirs: The view from the underside: Geology, v. 31, p. 849-852.
Erdős, Z., Beek, P. and Huismans, R.S., 2014, Evaluating balanced section restoration with thermochronology data: A case study from the Central Pyrenees: Tectonics, v. 33, p. 617-634.
Fan, G., Ni, J.F. and Wallace, T.C., 1994, Active tectonics of the Pamirs and Karakorum: Journal of Geophysical Research: Solid Earth, v. 99, p.7,131-7,160.
Farley, K.A., 2002, (U-Th)/He dating: Techniques, calibrations, and applications: Reviews in Mineralogy and Geochemistry, v. 47, p. 819-844.
Fillon, C., Huismans, R.S., and van der Beek, P., 2013, Syntectonic sedimentation effects on the growth of fold-and-thrust belts: Geology, v. 41, p. 83-86.
Forsyth, D., and Uyeda, S., 1975, On the relative importance of the driving forces of plate motion: Geophysical Journal International, v. 43, p. 163-200.
Fu, B., Ninomiya, Y., and Guo, J., 2010, Slip partitioning in the northeast Pamir-Tian Shan convergence zone: Tectonophysics, v. 483, p. 344-364.
Gagala, L., Ratschbacher, L., Ringenbach, J., Abdulhameed, S., Kässner, A., Szulc, A., Gloaguen, R., Rajabov, N. and Mirkamalov, R., 2014, Structure and exhumation ages of the Tajik Depression (western foreland of the Pamir): toward an integrated kinematic model: 14th International Conference on Thermochronology, Chamonix, France.
Gao, R., Hou, H., Cai, X., Knapp, J.H., He, R., Liu, J., Xiong, X., Guan, Y., Li, W., Zeng, L., and Roecker, S.W., 2013, Fine crustal structure beneath the junction of the southwest Tian Shan and Tarim Basin, NW China: Lithosphere, v. 5, p. 382-392.
Gilligan, A., Roecker, S.W., Priestley, K.F., and Nunn, C., 2014, Shear velocity model for the Kyrgyz Tien Shan from joint inversion of receiver function and surface wave data: Geophysical Journal International, v. 199, p. 480-498.
Gordon, S.M., Luffi, P., Hacker, B., Valley, J., Spicuzza, M., Kozdon, R., Kelemen, P., Ratshbacher, L. and Minaev, V., 2012, The thermal structure of continental crust in active orogens: insight from Miocene eclogite and granulite xenoliths of the Pamir Mountains: Journal of Metamorphic Geology, v. 30, p. 413-434.

Green, P.F., and Duddy, I.R., 1989, Some comments on paleotemperature estimation from apatite fission track analysis: Journal of Petroleum Geology, v. 12, p. 111-114.
Hacker, B., Luffi, P., Lutkov, V., Minaev, V., Ratschbacher, L., Plank, T., Ducea, M., Patiño-Douce, A., McWilliams, M., and Metcalf, J., 2005, Near-ultrahigh pressure processing of continental crust: Miocene crustal xenoliths from the Pamir: Journal of Petrology, v. 46, p.1,661-1,687.
Hamburger, M.W., Sarewitz, D.R., Pavlis, T.L. and Popandopulo, G.A., 1992, Structural and seismic evidence for intracontinental subduction in the Peter the First Range, central Asia: Geological Society of America Bulletin, v. 104, p. 397-408.
Heermance, R.V., Chen, J., Burbank, D. W., and Miao, J., 2008, Temporal constraints and pulsed Late Cenozoic deformation during the structural disruption of the active Kashi foreland, northwest China: Tectonics, v. 27.
Hendrix, M.S., Dumitru, T.A., and Graham, S.A.,1994, Late Oligocene–Early Miocene unroofing in the Chinese Tien Shan - an early effect of the India-Asian collision: Geology v. 22, p. 487–490.
Hossack, J.R., 1979, The use of balanced cross-sections in the calculation of orogenic contraction: A review: Journal of the Geological Society, v. 136, p. 705-711.
Hurford, A. J., and Green, P.F., 1983, The zeta age calibration of fission-track dating: Chemical Geology, v. 41, p. 285-317.
Ischuk, A., Bendick, R., Rybin, A., Molnar, P., Khan, S.F., Kuzikov, S., Mohadjer, S., Saydullaev, U., Ilyasova, Z., Schelochkov, G. and Zubovich, A.V., 2013, Kinematics of the Pamir and Hindu Kush regions from GPS geodesy: Journal of Geophysical Research: Solid Earth, v. 118, p.2,408-2,416.
Judge, P.A., and Allmendinger, R.W., 2011, Assessing uncertainties in balanced cross sections: Journal of Structural Geology, v. 33, p. 458-467.
Kapp, P., and Guynn, J.H., 2004, Indian punch rifts Tibet: Geology, v. 32, p. 993-996.
Kässner, A., Ratschbacher, L., Pfänder, J.A., Hacker, B.R., Zack, G., Sonntag, B.L., Khan, J., Stanek, K.P., Gadoev, M. and Oimahmadov, I., 2016, Proterozoic− Mesozoic history of the Central Asian orogenic belt in the Tajik and southwestern Kyrgyz Tian Shan: U-Pb, 40Ar/39Ar, and fission-track geochronology and geochemistry of granitoids: Geological Society of America Bulletin, B31466-1.
Ketcham, R.A., 1996, An improved method for determination of heat production with gamma-ray scintillation spectrometry: Chemical geology, v. 130, p. 175-194.
Ketcham, R.A., 2005, Forward and inverse modeling of low-temperature thermochronometry data: Reviews in mineralogy and geochemistry, v. 58, p. 275-314.
Ketcham, R.A., Carter, A., Donelick, R.A., Barbarand, J. and Hurford, A.J., 2007, Improved modeling of fission-track annealing in apatite: American Mineralogist, v. 92, p. 799-810.
Kley, J., 1996, Transition from basement-involved to thin-skinned thrusting in the Cordillera Oriental of southern Bolivia: Tectonics, v. 15, p. 763-775.
Klocke, M., Voigt, T., Kley, J., Pfeifer, S., Rocktäschel, T., Keil, S., and Gaupp, R., 2015, Cenozoic evolution of the Pamir and Tien Shan mountains reflected in syntectonic deposits of the Tajik Basin: Geological Society, London, Special Publications, v. 427.
Koulakov, I., and Sobolev, S.V., 2006, A tomographic image of Indian lithosphere break-off beneath the Pamir–Hindukush region: Geophysical Journal International, v. 164, p. 425-440.
Krystopowicz, N.J., and Currie, C.A., 2013, Crustal eclogitization and lithosphere delamination in orogens: Earth and Planetary Science Letters, v. 361, p. 195-207.
Kufner, S.K., Schurr, B., Sippl, C., Yuan, X., Ratschbacher, L., Ischuk, A., Murodkulov, S., Schneider, F., Mechie, J. and Tilmann, F., 2016, Deep India meets deep Asia: Lithospheric indentation, delamination and break-off under Pamir and Hindu Kush (Central Asia): Earth and Planetary Science Letters, v. 435, p.171-184.
Kumar, P., Yuan, X., Kind, R., and Kosarev, G., 2005, The lithosphere-asthenosphere boundary in the Tien Shan-Karakoram region from S receiver functions: Evidence for continental subduction: Geophysical Research Letters, v. 32.

Lei, J., 2011, Seismic tomographic imaging of the crust and upper mantle under the central and western Tien Shan orogenic belt: Journal of Geophysical Research, v. 116.

Leith, W., 1985, A Mid-Mesozoic extension across central Asia: Nature, v. 313, p. 567-570.

Leith, W., and Alvarez, W., 1985, Structure of the Vakhsh fold-and-thrust belt, Tadjik SSR: geologic mapping on a Landsat image base: Geological Society of America Bulletin, v. 96, p. 875–885.

Leven, E.Y., Leonova, T.B., and Dmitriev, V.Y., 1992, Permian of the Darvaz–Transalay Zone of Pamirs: Fusulinids, Ammonoids, Stratigraphy: Trudy Paleontologicheskogo Instituta RAN, v. 253, 197p.

Li, T., Chen, J., Thompson, J.A., Burbank, D.W. and Xiao, W., 2012, Equivalency of geologic and geodetic rates in contractional orogens: New insights from the Pamir Frontal Thrust: Geophysical Research Letters, v. 39.

Li, Z., Roecker, S.W., Li, Z., Wei, B., Wang, H., Schelochkov, G., and Bragin, V., 2009, Tomographic image of the crust and upper mantle beneath the western Tien Shan from the MANAS broadband deployment: Possible evidence for lithospheric delamination: Tectonophysics, v. 477, p. 49–57.

Lock, J., and Willett, S., 2008, Low-temperature thermochronometric ages in fold-and-thrust belts: Tectonophysics, v. 456, p. 147-162.

Lukens, C.E., Carrapa, B., Singer, B.S. and Gehrels, G., 2012, Miocene exhumation of the Pamir revealed by detrital geothermochronology of Tajik rivers: Tectonics, v. 31.

Mahéo, G., Guillot, S., Blichert-Toft, J., Rolland, Y. and Pêcher, A., 2002, A slab breakoff model for the Neogene thermal evolution of South Karakorum and South Tibet: Earth and Planetary Science Letters, v. 195, p. 45-58.

Makarov, V.I., Alekseev, D.V., Batalev, V.Y., Bataleva, E.A., Belyaev, I.V., Bragin, V.D., Dergunov, N.T., Efimova, N.N., Leonov, M.G., Munirova, L.M. and Pavlenkin, A.D., 2010, Underthrusting of Tarim beneath the Tien Shan and deep structure of their junction zone: Main results of seismic experiment along MANAS Profile Kashgar-Song-Köl: Geotectonics, v. 442, p. 102-126.

Mareschal, J.C. and Jaupart, C., 2013, Radiogenic heat production, thermal regime and evolution of continental crust: Tectonophysics, v. 609, p. 524-534.

McQuarrie, N. and Ehlers, T.A., 2015, Influence of thrust belt geometry and shortening rate on thermochronometer cooling ages: Insights from thermokinematic and erosion modeling of the Bhutan Himalaya: Tectonics, v. 34, p. 1055-1079.

McQuarrie, N., 2004, Crustal scale geometry of the Zagros fold–thrust belt, Iran: Journal of Structural Geology, v. 26, p. 519-535.

Mechie, J., Yuan, X., Schurr, B., Schneider, F., Sippl, C., Ratschbacher, L., Minaev, V., Gadoev, M., Oimahmadov, I., Abdybachaev, U. and Moldobekov, B., 2012, Crustal and uppermost mantle velocity structure along a profile across the Pamir and southern Tien Shan as derived from project TIPAGE wide-angle seismic data: Geophysical Journal International, v. 188, p. 385-407.

Mesezhnikov, M.S., 1988, Oxforidian, *in* Mesezhnikov, M.S., and Westermann, G.E.G., eds., The Jurassic Ammonite Zones of the Soviet Union: Geological Society of America Special Papers, v. 223, 116p.

Mitra, S. and Namson, J.S., 1989, Equal-area balancing: American Journal of Science, v. 289, p. 563-599.

Mitra, S., 2002, Structural models of faulted detachment folds: American Association of Petroleum Geologists Bulletin, v. 86, p. 1,673-1,694.

Mohadjer, S., Bendick, R., Ischuk, A., Kuzikov, S., Kostuk, A., Saydullaev, U., Lodi, S., Kakar, D.M., Wasy, A., Khan, M.A., Molnar, P., Bilham, R., and Zubovich, A.V., 2010, Partitioning of India–Eurasia convergence in the Pamir–Hindu Kush from GPS measurements: Geophysical Research Letters, v. 37, p. 1–6.

Molnar, P. and Gray, D., 1979. Subduction of continental lithosphere: Some constraints and uncertainties: Geology, v. 7, p. 58-62.

Molnar, P. and Lyon-Caen, H., 1988, Some simple physical aspects of the support, structure, and evolution of mountain belts: Geological Society of America Special Papers, v. 218, p. 179-208.

Molnar, P., 2004, Late Cenozoic increase in accumulation rates of terrestrial sediment: How might climate change have affected erosion rates?: Annual Review of Earth and Planetary Sciences, v. 32, p. 67-89.

Molnar, P., and Stock, J.M., 2009, Slowing of India's convergence with Eurasia since 20 Ma and its implications for Tibetan mantle dynamics: Tectonics, v. 28, TC3001.

Molnar, P., and Tapponnier, P., 1975, Cenozoic tectonics of Asia: Effect of a continental collision: Science, v. 189, p. 419–426.

Molnar, P., and Tapponnier, P., 1981, A possible dependence of tectonic strength on the age of the crust in Asia: Earth and Planetary Science Letters, v. 52, p. 107-114.

Mora, A., Casallas, W., Ketcham, R.A., Gomez, D., Parra, M., Namson, J., Stockli, D., Almendral, A., Robles, W. and Ghorbal, B., 2015, Kinematic restoration of contractional basement structures using thermokinematic models: A key tool for petroleum system modeling: American Association of Petroleum Geologists Bulletin, v. 99, p. 1575-1598.

Morgan, W.J., 1965, Gravity anomalies and convection currents. 1. A sphere and cylinder sinking beneath the surface of a viscous fluid: Journal of Geophysical Research v. 70, p. 6175-6187.

Negredo, A.M., Replumaz, A., Villaseñor, A. and Guillot, S., 2007, Modeling the evolution of continental subduction processes in the Pamir–Hindu Kush region: Earth and Planetary Science Letters, v. 259, p. 212-225.

Nikolaev, V.G., 2002, Afghan-Tajik depression: Architecture of sedimentary cover and evolution: Russian Journal of Earth Sciences, v. 4, p. 399-421.

Pavlis, G.L., and Das, S., 2000, The Pamir-Hindu Kush seismic zone as a strain marker for flow in the upper mantle: Tectonics, v. 19, p. 103-115.

Pavlis, T.L., Hamburger, M. W., and Pavlis, G.L., 1997, Erosional processes as a control on the structural evolution of an actively deforming fold and thrust belt: An example from the Pamir-Tien Shan region, central Asia: Tectonics, v. 16, p. 810-822.

Pegler, G., and Das, S., 1998,. An enhanced image of the Pamir–Hindu Kush seismic zone from relocated earthquake hypocentres: Geophysical Journal International, v. 134, p. 573-595.

Pozzi, J.P., and Feinberg, H., 1991, Paleomagnetism in the Tajikistan: Continental shortening of European margin in the Pamirs during Indian Eurasian collision: Earth and Planetary Science Letters, v. 103, p. 365-378.

Price, R.A., 1986, The southeastern Canadian Cordillera: thrust faulting, tectonic wedging, and delamination of the lithosphere: Journal of Structural Geology, v. 8, p. 239-254.

Price, R.A., and Mountjoy, E.W., 1970, Geologic structure of the Canadian Rocky mountains between Bow and Athabasca rivers, a progress report, *in* Wheeler, J.O., ed., Structure of the Southern Canadian Cordillera: Geological Association of Canada, p. 7-25.

Qiu, N., Chang, J., Zuo, Y., Wang, J. and Li, H., 2012, Thermal evolution and maturation of lower Paleozoic source rocks in the Tarim Basin, northwest China: American Association of Petroleum Geologists Bulletin, v.96, p. 789-821.

Ramsay, J.G., and Huber, M.I., 1987, The techniques of modern structural geology, volume 2: folds and fractures: Academic press, 391p.

Reiners, P.W., and Brandon, M.T., 2006, Using thermochronology to understand orogenic erosion: Annual Review of Earth and Planetary Sciences, v. 34, p. 419-466.

Reiners, P.W., Spell, T., Nicolescu, S., Zanetti, K., 2004, Zircon (U–Th)/He thermochronometry: He diffusion and comparisons with $^{40}Ar/^{39}Ar$ dating: Geochimica et cosmochimica acta, v. 68, p. 1,857-1,887.

Reiter, K., Kukowski, N., and Ratschbacher, L., 2011, The interaction of two indenters in analogue experiments and implications for curved fold-and-thrust belts: Earth and Planetary Science Letters, v. 302, p. 132-146.

Replumaz, A., Negredo, A.M., Guillot, S., and Villaseñor, A., 2010, Multiple episodes of continental subduction during India/Asia convergence: Insight from seismic tomography and tectonic reconstruction: Tectonophysics, v. 483, p. 125-134.

Robinson, A.C., 2015, Mesozoic tectonics of the Gondwanan terranes of the Pamir plateau: Journal of Asian Earth Sciences, v. 102, p. 170-179.
Robinson, A.C., Ducea, M. and Lapen, T.J., 2012, Detrital zircon and isotopic constraints on the crustal architecture and tectonic evolution of the northeastern Pamir: Tectonics, v. 31.
Robinson, D.M. and McQuarrie, N., 2012, Pulsed deformation and variable slip rates within the central Himalayan thrust belt: Lithosphere, v. 4, p. 449-464.
Roecker, S.W., 1982, Velocity structure of the Pamir-Hindu Kush Region: Possible evidence of subducted crust: Journal of Geophysical Research: Solid Earth, v. 87, p. 945-959.
Roecker, S.W., Sabitova, T.M., Vinnik, L.P., Burmakov, Y.A., Golvanov, M.I., Mamatkanova, R., and Munirova, L., 1993, Three-dimensional elastic wave velocity structure of the western and central Tien Shan: Journal of Geophysical Research: Solid Earth, v. 98, p. 15,779-15,795.
Rudnick R.L. and Gao, S., 2003, Composition of the continental crust: in The Crust, v. 3, Elsevier, p. 1-64.
Rutte, D., Stearns, M., and Ratschbacher, L., 2013, The eastern Central Pamir Gneiss Domes: temporal and spatial geometry of burial and exhumation: European Geophysical Union General Assembly Conference Abstracts, v. 15, p. 6,090.
Scharer, K.M., Burbank, D.W., Chen, J., Weldon, R.J., Rubin, C., Zhao, R., and Shen, J, 2004, Detachment folding in the Southwestern Tian Shan–Tarim foreland, China: shortening estimates and rates: Journal of Structural Geology, v. 26, p. 2,119-2,137.
Schellart, W.P., 2008, Subduction zone trench migration: Slab driven or overriding-plate-driven?: Physics of the Earth and Planetary Interiors, v. 170, p. 73-88.
Schmidt, J., Hacker, B.R., Ratschbacher, L., Stübner, K., Stearns, M., Kylander-Clark, A., Cottle, J.M., Alexander, A., Webb, G., Gehrels, G. and Minaev, V., 2011, Cenozoic deep crust in the Pamir: Earth and Planetary Science Letters, v. 312, p. 411-421.
Schneider, F.M., Yuan, X., Schurr, B., Mechie, J., Sippl, C., Haberland, C., Minaev, V., Oimahmadov, I., Gadoev, M., Radjabov, N. and Abdybachaev, U., 2013, Seismic imaging of subducting continental lower crust beneath the Pamir: Earth and Planetary Science Letters, v. 375, p. 101-112.
Schurr, B., Ratschbacher, L., Sippl, C., Gloaguen, R., Yuan, X., and Mechie, J., 2014, Seismotectonics of the Pamir: Tectonics, v. 33, p. 1,501-1,518.
Schwab, M., Ratschbacher, L., Siebel, W., McWilliams, M., Minaev, V., Lutkov, V., Chen, F., Stanek, K., Nelson, B., Frisch, W. and Wooden, J.L., 2004, Assembly of the Pamirs: Age and origin of magmatic belts from the southern Tien Shan to the southern Pamirs and their relation to Tibet: Tectonics, v. 23.
Sippl, C., Schurr, B., Yuan, X., Mechie, J., Schneider, F.M., Gadoev, M., Orunbaev, S., Oimahmadov, I., Haberland, C., Abdybachaev, U. and Minaev, V., 2013, Geometry of the Pamir-Hindu Kush intermediate-depth earthquake zone from local seismic data: Journal of Geophysical Research: Solid Earth, v. 118, p. 1,438-1,457.
Smit, M.A., Ratschbacher, L., Kooijman, E., and Stearns, M.A., 2014, Early evolution of the Pamir deep crust from Lu-Hf and U-Pb geochronology and garnet thermometry: Geology, v. 42, p. 1,047-1,050.
Sobel, E.R. and Dumitru, T.A., 1997, Thrusting and exhumation around the margins of the western Tarim basin during the India-Asia collision: Journal of Geophysical Research: Solid Earth, v. 102, p. 5,043-5,063.
Sobel, E.R., Chen, J., and Heermance, R.V., 2006, Late Oligocene–early Miocene initiation of shortening in the southwestern Chinese Tian Shan: Implications for Neogene shortening rate variations: Earth and Planetary Science Letters, v. 247, p. 70–81.
Sobel, E.R., Chen, J., Schoenbohm, L.M., Thiede, R., Stockli, D F., Sudo, M., and Strecker, M.R., 2013, Oceanic-style subduction controls late Cenozoic deformation of the Northern Pamir orogen: Earth and Planetary Science Letters, v. 363, p. 204-218.

Sobolev, S.V., Babeyko, A.Y., Koulakov, I., and Oncken, O., 2006, Mechanism of the Andean orogeny: insight from numerical modeling, *in*, Oncken, O., Chong, G., Franz, G., Giese, P., Götze, H-J.,. Ramos, V., Strecker, M.R., and Wigger, P., eds., The Andes: Springer, Berlin Heidelberg, p. 513-535.

Stearns, M.A., Hacker, B.R., Ratschbacher, L., Lee, J., Cottle, J.M., and Kylander-Clark, A., 2013, Synchronous Oligocene–Miocene metamorphism of the Pamir and the north Himalaya driven by plate-scale dynamics: Geology, v. 41, p. 1,071-1,074.

Stearns, M.A., Hacker, B.R., Ratschbacher, L., Rutte, D. and Kylander-Clark, A.R.C., 2015, Titanite petrochronology of the Pamir gneiss domes: Implications for middle to deep crust exhumation and titanite closure to Pb and Zr diffusion: Tectonics, v. 34, p. 784-802.

Stockmal, G.S., Beaumont, C., Nguyen, M., and Lee, B., 2007, Mechanics of thin-skinned fold-and-thrust belts: Insights from numerical models: Geological Society of America Special Papers, v. 433, p. 63-98.

Strecker, M.R., Hilley, G.E., Arrowsmith, J.R., and Coutand, I., 2003, Differential structural and geomorphic mountain-front evolution in an active continental collision zone: The northwest Pamir, southern Kyrgyzstan: Geological Society of America Bulletin, v. 115, p. 166-181.

Stübner, K., Ratschbacher, L., Rutte, D., Stanek, K., Minaev, V., Wiesinger, M., and Gloaguen, R., 2013a, The giant Shakhdara migmatitic gneiss dome, Pamir, India-Asia collision zone: 1. Geometry and kinematics: Tectonics, v. 32, p. 948-979.

Stübner, K., Ratschbacher, L., Weise, C., Chow, J., Hofmann, J., Khan, J., Rutte, D., Sperner, B., Pfänder, J.A., Hacker, B.R. and Dunkl, I., 2013b, The giant Shakhdara migmatitic gneiss dome, Pamir, India-Asia collision zone: 2. Timing of dome formation: Tectonics, v. 32, p. 1404-1431.

Sun, J., Li, Y., Zhang, Z., and Fu, B., 2009, Magnetostratigraphic data on Neogene growth folding in the foreland basin of the southern Tianshan Mountains: Geology, v. 37, p. 1,051-1,054.

Tapponnier, P., and Molnar, P., 1979, Active faulting and Cenozoic tectonics of the Tien Shan, Mongolia, and Baykal regions: Journal of Geophysical Research, v. 84, p. 3,425–3,459.

Thomas, J.-C., Chauvin, A., Gapais, D., Bazhenov, M.L., Perroud, H., Cobbold, P.R., and Burtman, V.S., 1994, Paleomagnetic evidence for Cenozoic block rotations in the Tadjik Depression (Central Asia): Journal of Geophysical Resesarch, v. 99, p. 15,141–15,160.

Thompson, J.A., Burbank, D.W., Li, T., Chen, J., and Bookhagen, B., 2015, Late Miocene northward propagation of the northeast Pamir thrust system, northwest China: Tectonics, v. 34, p. 510-534.

Trifonov, V.G., 1978, Late Quaternary tectonic movements of western and central Asia: Geological Society of America Bulletin, v. 89, p. 1,059-1,072.

Turcotte, D.L., and Schubert, G., 2014, Geodynamics. Cambridge University Press, 636p.

Ulmishek, G.F., 2004, Petroleum geology and resources of the Amu-Darya basin, Turkmenistan, Uzbekistan, Afghanistan, and Iran: United States Geological Survey Bulletin 2201-H.

Vann, I.R., Graham, R.H., and Hayward, A.B., 1986, The structure of mountain fronts: Journal of Structural Geology, v. 8, p. 215-227.

Vlasov, N., Yu, G., Dyakov, A., and Cherev E.S., 1991, Geological map of the Tajik SSR and adjacent territories, 1:500,000: Vsesojuznoi Geologic Institute of Leningrad, Saint Petersburg.

Wang, X., Flynn, L.J., and Fortelius, M., editors, 2013, Fossil mammals of Asia: Neogene biostratigraphy and chronology: Columbia University Press, 752p.

Wells, M.L., Hoisch, T.D., Cruz-Uribe, A.M., and Vervoort, J.D., 2012, Geodynamics of synconvergent extension and tectonic mode switching: Constraints from the Sevier-Laramide orogen: Tectonics, v. 31, TC1002.

Whipp, D.M., Ehlers, T.A., Blythe, A.E., Huntington, K.W., Hodges, K.V. and Burbank, D.W., 2007, Plio-Quaternary exhumation history of the central Nepalese Himalaya: 2. Thermokinematic and thermochronometer age prediction model: Tectonics, v. 26.

Windley, B.F., Allen, M.B., Zhang, C., Zhao, Z.Y., and Wang, G.R., 1990, Paleozoic accretion and Cenozoic redeformation of the Chinese Tien Shan range, central Asia: Geology v. 18, p. 128–131.

Woodward, N.B., Boyer, S.E., and Suppe, J., 1989, Balanced Geological Cross sections: an essential technique in geological research and exploration: American Geophysical Union, Washington, D.C., p.170.

Yin, A., Nie, S., Craig, P., Harrison, T.M., Ryerson, F.J., Xianglin, Q., and Geng, Y., 1998, Late Cenozoic tectonic evolution of the southern Chinese Tian Shan: Tectonics, v. 17, p. 1-27.

Figure Captions

1. Overview map of the Southern Tian Shan and Pamir Mountains region. Lower panels: schematic end-member models for the origin of the Pamir Seismic Zone (PSZ) as it is observed today (models are not to scale). A) Overturned slab of subducted Indian lithosphere, with small rotational arrows showing overturning of the portion of the slab that has broken off (e.g., Koulakov and Sobolev, 2006). B) Subduction of Asian lithosphere (e.g., Schneider et al., 2013; Sippl et al., 2013), that may have initially been subducted at a low-angle and then rolled back to the north (e.g. Sobel et al., 2013; Stearns et al., 2015). C) Delamination of Pamir lithosphere (Stearns et al., 2015; Kufner et al., 2016; Rutte et al., 2017b, this study). Previously detached portions of the Indian lithosphere (e.g., Mahéo et al., 2002) are not shown in panels B or C. MPT=Main Pamir Thrust, DF=Darvaz Fault, TBZ=Tirich-Mir Fault Zone, MBT=Main Boundary Thrust, CHMF=Chaman Fault, PFR=Peter the First Range, FTB=Fold and Thrust Belt.

2. Geologic Map of the northern Tajik Basin and Tajik Fold and Thrust Belt. Cross-section A-A' is presented in Figure 3A and cross-section B-B' in presented in Figure 3D. Geology is modified from (Vlasov et al., 1991). Thermochronological sample information is presented in Table 1. AHe=apatite (U-Th)/He, AFT=apatite fission track, DF=Darvaz fault, MPT=Main Pamir thrust, NMPT = north MPT, SMPT = south MPT, DSZ = Dashtak shear zone, TMS = Tanymas suture, YGD = Yazgulem gneiss dome. Stratigraphic nomenclature adopted from Burtman (2000) and Nikolaev (2002). AHe ages are weighted means.

3. A) Cross-section A-A', see Figure 2 for location. Well names for wells plotted in cross-section A-A' are 1) Yakkasaray-6, 2) Mirshadi-1, 3) Kurgancha-21, 4) Beshtentyak-22. B) Restoration of cross-section A-A' from panel A. C) Close-up of cross-section A-A' across the Tajik fold and thrust belt (TFTB) that is basis for subsequent FETKin modeling. Compare panel C to the 0 Ma (fully deformed) section in Figure 5 and Figure 6C. Sample locations and structural (dip) data were projected from along strike and plotted at correlative structural level. D) Cross-section B-B', see Figure 2 for location. A portion of the section in the Peter 1st Range is based on Hamburger et al. (1992). E) Restoration of cross-section B-B' from panel D. The colors and labels for geologic features in all panels is the same as in Figure 2. DF = Darvaz fault, PFT = Pamir frontal thrust, MPT = Main Pamir thrust, NMPT = north MPT, SMPT = south MPT, DSZ = Dashtak shear zone, TMS = Tanymas suture.

4. Results from flexural modeling that suggests some of the structural relief on the Jurassic décollement can be explained by lithospheric loading associated with the Tian Shan and Pamir. The actual elevation of the Jurassic décollement is 3.3 km lower (the thickness of the Miocene and younger sedimentary section).

5. Sequential cross-sections from 20 Ma to 0 Ma. These sections were forward modeled in MOVE and then imported into FETKin and form the basis for the preferred, baseline model. Compare the geometry in the 0Ma section to Figure 3C. Structures are labeled in

the time step at which they become active in the model. Note subsidence at each time step in the model, which is based on flexural modeling (Fig. 4).

6. Predicted (modeled) AHe and AFT ages compared against measured cooling ages from Table 1. Preferred model refers to the baseline model. All modeled ages have a prescribed inherited age of 30 Ma. Deformation appears to propagate towards the center of the Tajik fold and thrust belt. A) Preferred model cooling ages compared to predicted ages from models with higher or lower prescribed basal temperature. B) Preferred model cooling ages compared to predicted ages from models with slip on each individual structure moved forward (late model) or back (early model) in time by 2 Myr. C) Close-up of the final (0 Ma) model geometry used in FETKin modeling. Compare to Figure 3C.

7. A) Geothermal gradient vs. distance in the upper 10 km of the final time step (0 Ma) in FETKin models with varying basal temperatures. The geothermal gradient profile for the 500°C basal temperature corresponds to the preferred baseline model and is located almost entirely within the estimated range of modern geothermal gradients. B) Isotherms for the preferred baseline model showing their deflection resulting from the advection and deposition of material in the FETkin modeling.

8. Photo of Neogene growth strata located just west of the large overturned synclinorium in the Dashtijum Valley region. Location: 37.85°N, 69.95°E.

9. Plot of cumulative shortening in the Tajik fold and thrust belt based on FETKin model results for the preferred baseline model and models in which slip on individual structures was moved forward (late model) or backward (early model) in time. Results from early and late models are only plotted when the predicted AHe and AFT cooling ages fall within error of the measured cooling ages (Fig. 6B). The results indicate Miocene to present shortening rates of 4-6 mm/yr.

10. A series of cartoon cross-sections across the A) Tajik Basin, B) Alai Valley, and C) Tarim Basin that show how shortening and deformation may have evolved to produce the bivergent structural geometries (structures on opposite margins of the basins verging inward toward the center of the basin) observed in the Tajik fold and thrust belt (TFTB). The total amount of shortening in each section is comparable. TS=Tian Shan.

11. A schematic cross-section across the Tian Shan, Pamir, and Himalaya showing delamination of the Pamir mantle lithosphere and lower crust. Arrows in the Northern Pamir terrane indicate underthrusting of Tajik Basin/Northern Pamir lithosphere beneath the Pamir and Tian Shan. Seismicity and Moho locations are from Mechie et al. (2012) and Schneider et al. (2013). Himalayan thrust belt and Kohistan geometry modified from DiPietro and Pogue (2004) and Burg (2011). MPT=Main Pamir Thrust, SPB=South Pamir Batholith, KKB=Karakoram Batholith, KHB=Kohistan Batholith, MBT=Main Boundary Thrust, MFT=Main Frontal Thrust, CML=Continental Mantle Lithosphere.

Table Captions

Table 1. For AHe aliquots from the same sample, we report a weighted mean age and 2 sigma weighted uncertainty or a 1 sigma age standard deviation, whichever uncertainty is larger. #gr = number of grain analyses included in AHe age. AFT ages are central ages with 2 sigma uncertainty.

Table 2. Each column is a time step (Ma) in the preferred (baseline) thermokinematic model. The value in each cell is the amount of displacement (km) for a particular structure at that time step. For example, we modeled 3 km of slip on the Rangon thrust at the 12 Ma to 10 Ma time step. The total amount of slip on each structure is shown in the right-hand column. The total amount of slip for each time step is shown in the bottom row. These slip values produced the model geometries presented in Figure 5.

Supplementary Information

Table S1. Flexural parameters for modeling .

Table S2. Apatite (U-Th)/He (AHe) data for individual aliquots.

Table S3. Apatite fission track (AFT) data for samples analyzed.

Figure S1. Bottom hole temperature plotted against well-depth to estimate modern geothermal gradient.

Figure S2. Apatite (U-Th)/He (AHe) ages for individual aliquots of each sample plotted against effective uranium concentration (eU).

File S1. Matlab script for modeling plate flexure with spatially variable flexural rigidity using a centered-difference approach.

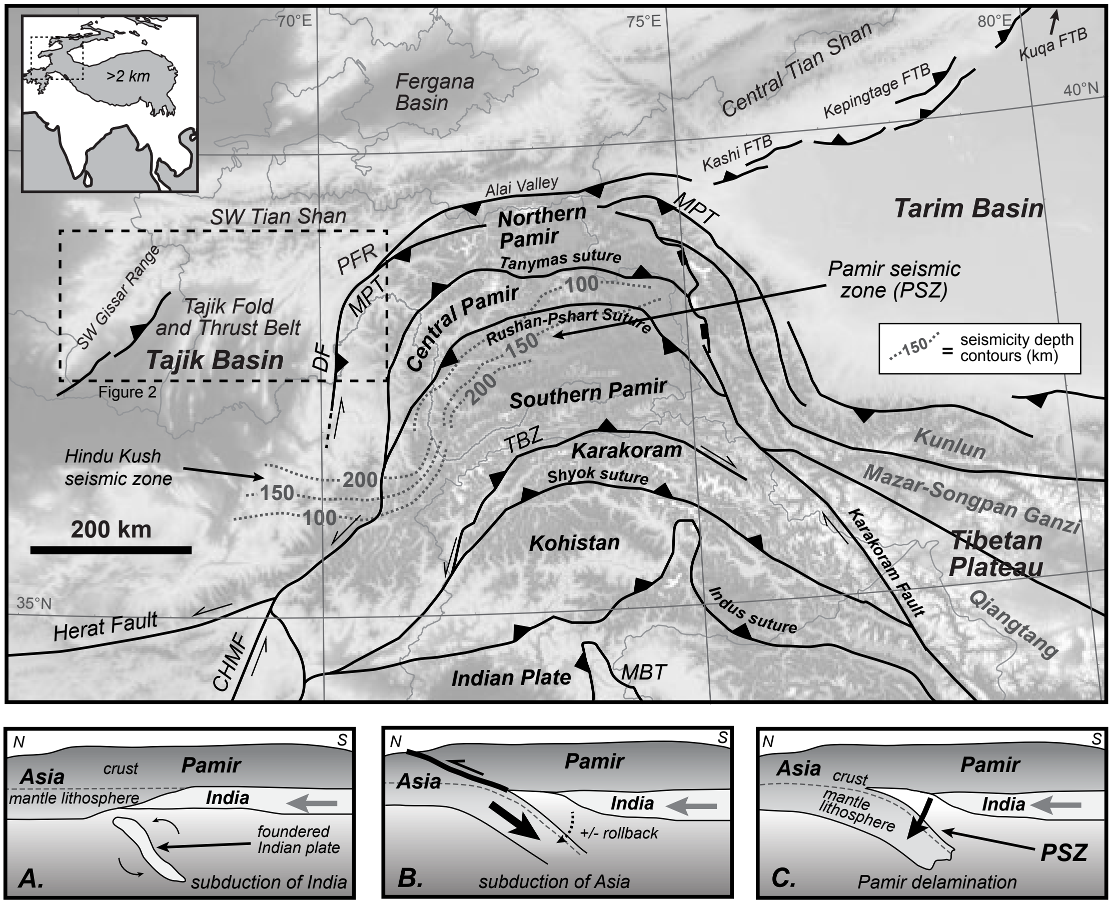
Fergana Basin
Central Tian Shan
Kuqa FTB
Kepingtage FTB
Kashi FTB
Tarim Basin
Alai Valley
SW Tian Shan
Northern Pamir
MPT
PFR
Tanymas suture
Pamir seismic zone (PSZ)
SW Gissar Range
Tajik Fold and Thrust Belt
Tajik Basin
Figure 2
DF
Central Pamir
Rushan-Pshart Suture
seismicity depth contours (km)
Southern Pamir
TBZ
Karakoram
Shyok suture
Kunlun
Mazar-Songpan Ganzi
Tibetan Plateau
Qiangtang
Hindu Kush seismic zone
200 km
Kohistan
Karakoram Fault
Indus suture
Herat Fault
CHMF
Indian Plate
MBT
>2 km
70°E
75°E
80°E
40°N
35°N
Asia
crust
Pamir
mantle lithosphere
India
founded Indian plate
subduction of India
A.
+/- rollback
subduction of Asia
B.
PSZ
Pamir delamination
C.

Figure 1

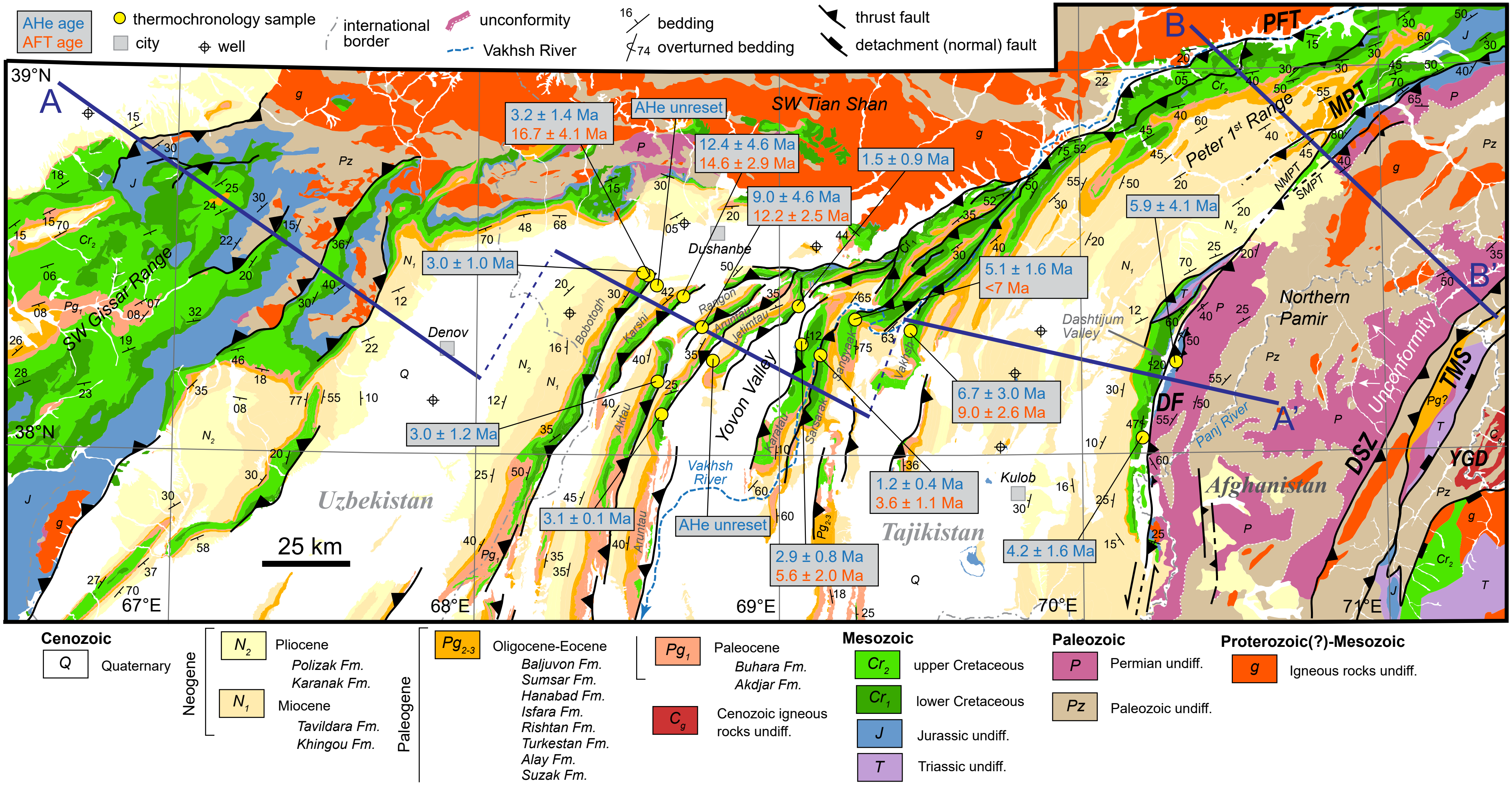
AHe age
AFT age
thermochronology sample
city
well
international border
unconformity
Vakhsh River
bedding
overturned bedding
thrust fault
detachment (normal) fault
39°N
38°N
67°E
68°E
69°E
70°E
71°E
A
A'
B
B'
SW Tian Shan
SW Gissar Range
Peter 1st Range
Northern Pamir
Dushanbe
Denov
Kulob
Dashtijum Valley
Yovon Valley
Vakhsh River
Panj River
Uzbekistan
Tajikistan
Afghanistan
Unconformity
PFT
MPT
NMPT
SMPT
DF
DSZ
TMS
YGD
Bobotogh
Karshi
Aktau
Aruntau
Rangon
Teletau
Jetimtau
Karatau
Sarsarak
Sangvorak
Vakhsh
25 km
3.2 ± 1.4 Ma
16.7 ± 4.1 Ma
AHe unreset
12.4 ± 4.6 Ma
14.6 ± 2.9 Ma
1.5 ± 0.9 Ma
9.0 ± 4.6 Ma
12.2 ± 2.5 Ma
5.9 ± 4.1 Ma
3.0 ± 1.0 Ma
5.1 ± 1.6 Ma
<7 Ma
6.7 ± 3.0 Ma
9.0 ± 2.6 Ma
3.0 ± 1.2 Ma
1.2 ± 0.4 Ma
3.6 ± 1.1 Ma
3.1 ± 0.1 Ma
AHe unreset
2.9 ± 0.8 Ma
5.6 ± 2.0 Ma
4.2 ± 1.6 Ma
Cenozoic
Q
Quaternary
Neogene
N2
Pliocene
Polizak Fm.
Karanak Fm.
N1
Miocene
Tavildara Fm.
Khingou Fm.
Paleogene
Pg2-3
Oligocene-Eocene
Baljuvon Fm.
Sumsar Fm.
Hanabad Fm.
Isfara Fm.
Rishtan Fm.
Turkestan Fm.
Alay Fm.
Suzak Fm.
Pg1
Paleocene
Buhara Fm.
Akdjar Fm.
Cg
Cenozoic igneous rocks undiff.
Mesozoic
Cr2
upper Cretaceous
Cr1
lower Cretaceous
J
Jurassic undiff.
T
Triassic undiff.
Paleozoic
P
Permian undiff.
Pz
Paleozoic undiff.
Proterozoic(?)-Mesozoic
g
Igneous rocks undiff.

Figure 2

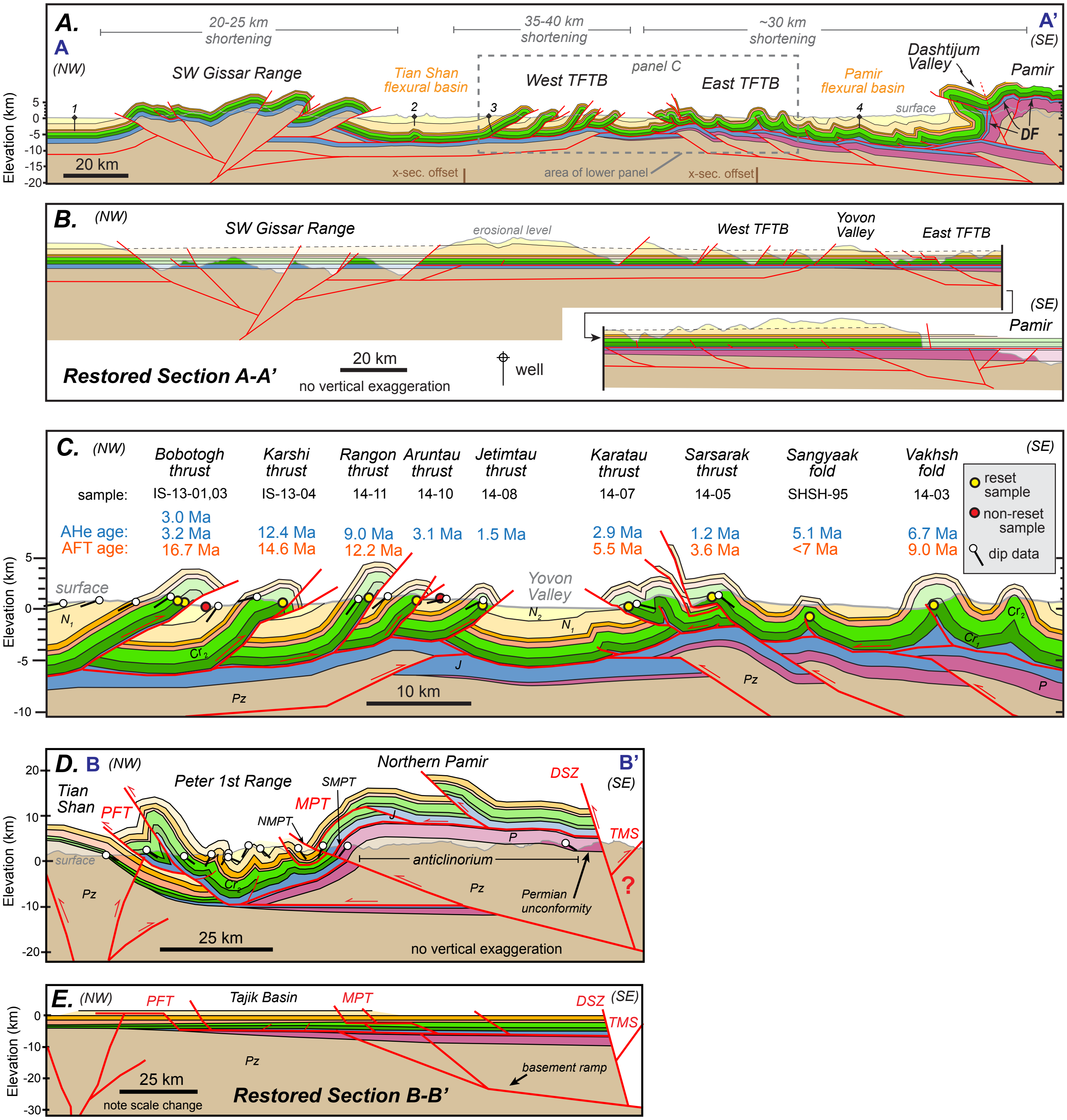

A.
A
(NW)
20-25 km shortening
35-40 km shortening
~30 km shortening
A'
(SE)
SW Gissar Range
Tian Shan flexural basin
panel C
West TFTB
East TFTB
Pamir flexural basin
Dashtijum Valley
Pamir
surface
DF
20 km
x-sec. offset
area of lower panel
Elevation (km)
B.
(NW)
SW Gissar Range
erosional level
West TFTB
Yovon Valley
East TFTB
(SE)
Pamir
Restored Section A-A'
20 km
no vertical exaggeration
well
C.
(NW)
Bobotogh thrust
Karshi thrust
Rangon thrust
Aruntau thrust
Jetimtau thrust
Karatau thrust
Sarsarak thrust
Sangyaak fold
Vakhsh fold
(SE)
sample:
IS-13-01,03
IS-13-04
14-11
14-10
14-08
14-07
14-05
SHSH-95
14-03
AHe age:
AFT age:
3.0 Ma
3.2 Ma
16.7 Ma
12.4 Ma
14.6 Ma
9.0 Ma
12.2 Ma
3.1 Ma
1.5 Ma
2.9 Ma
5.5 Ma
1.2 Ma
3.6 Ma
5.1 Ma
<7 Ma
6.7 Ma
9.0 Ma
reset sample
non-reset sample
dip data
surface
Yovon Valley
10 km
D.
B
(NW)
Tian Shan
PFT
Peter 1st Range
Northern Pamir
SMPT
NMPT
MPT
DSZ
B'
(SE)
TMS
surface
anticlinorium
Permian unconformity
25 km
no vertical exaggeration
E.
(NW)
PFT
Tajik Basin
MPT
DSZ
(SE)
TMS
basement ramp
25 km
note scale change
Restored Section B-B'

Figure 3

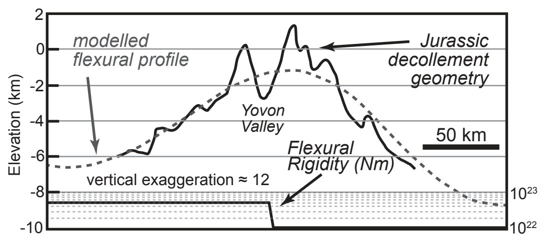

2
0
-2
-4
-6
-8
-10
Elevation (km)
modelled
flexural profile
Jurassic
decollement
geometry
Yovon
Valley
50 km
Flexural
Rigidity (Nm)
vertical exaggeration ≈ 12
10^23
10^22

Figure 4

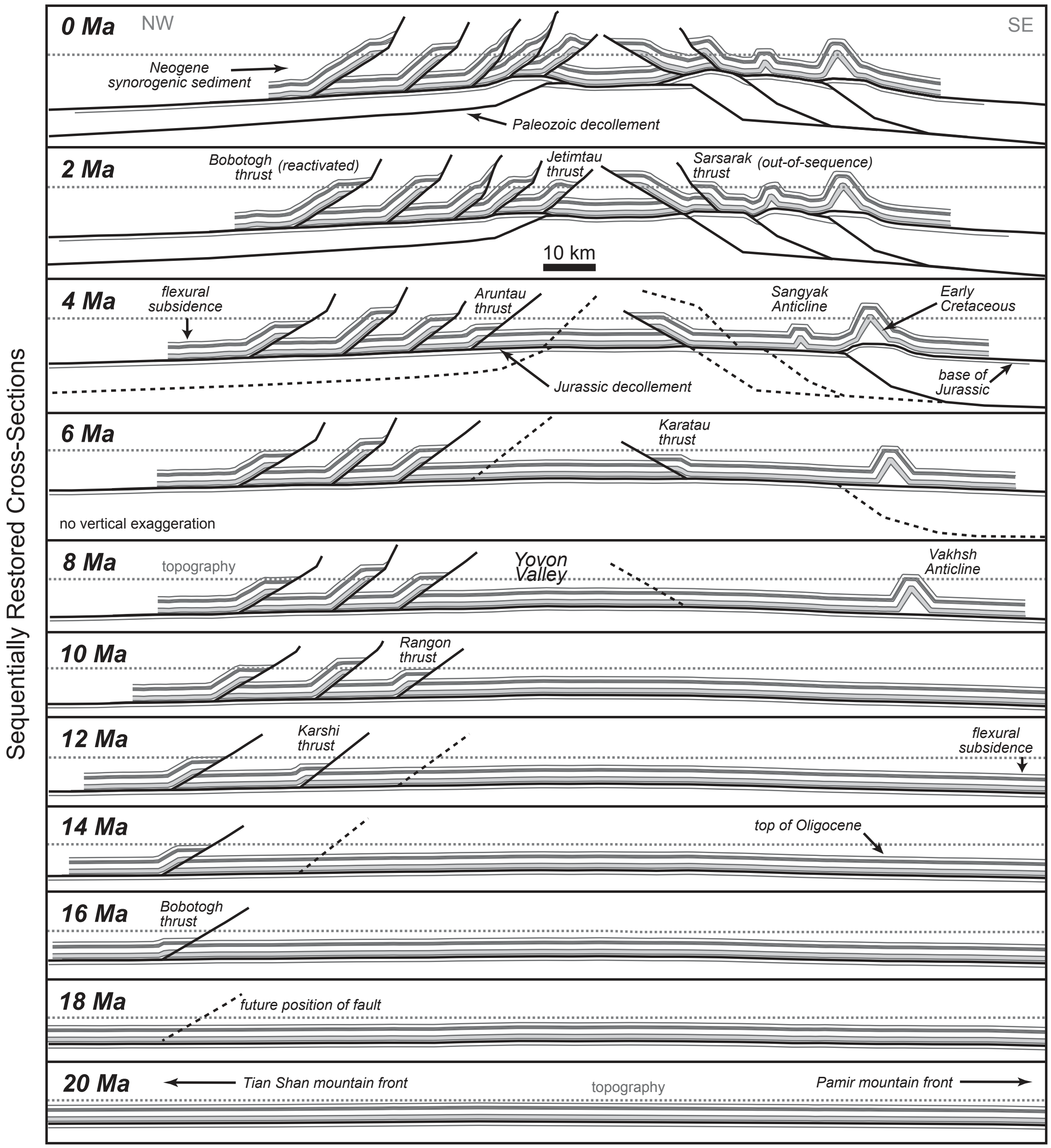
Sequentially Restored Cross-Sections
0 Ma
NW
SE
Neogene
synorogenic sediment
Paleozoic decollement
2 Ma
Bobotogh
thrust
(reactivated)
Jetimtau
thrust
Sarsarak
thrust
(out-of-sequence)
10 km
4 Ma
flexural
subsidence
Aruntau
thrust
Sangyak
Anticline
Early
Cretaceous
Jurassic decollement
base of
Jurassic
6 Ma
Karatau
thrust
no vertical exaggeration
8 Ma
topography
Yovon
Valley
Vakhsh
Anticline
10 Ma
Rangon
thrust
12 Ma
Karshi
thrust
flexural
subsidence
14 Ma
top of Oligocene
16 Ma
Bobotogh
thrust
18 Ma
future position of fault
20 Ma
Tian Shan mountain front
topography
Pamir mountain front

Figure 05

Figure 06

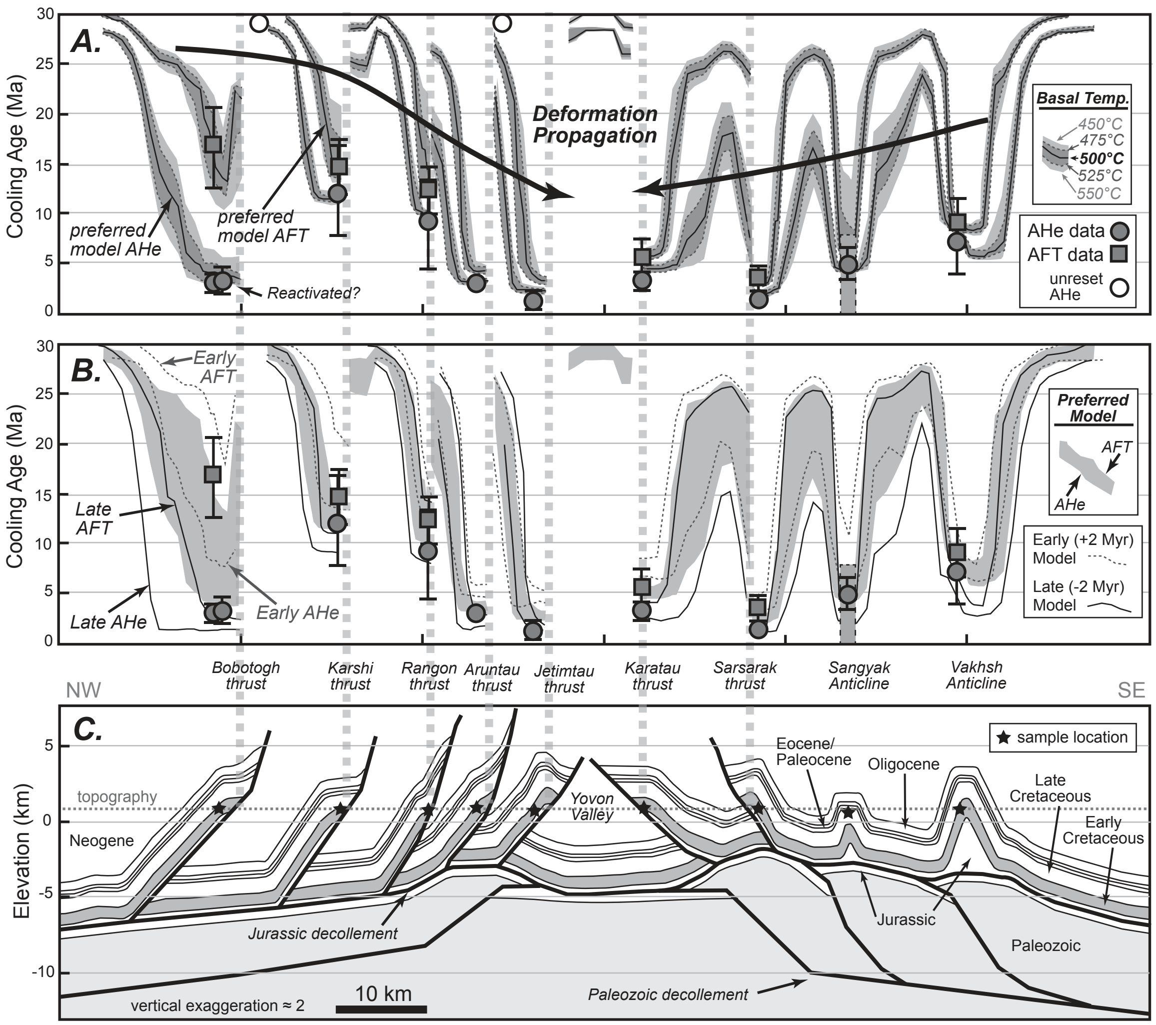

A.
Cooling Age (Ma)
Deformation Propagation
preferred model AHe
preferred model AFT
Reactivated?
Basal Temp.
450°C
475°C
500°C
525°C
550°C
AHe data
AFT data
unreset AHe
B.
Early AFT
Late AFT
Late AHe
Early AHe
Preferred Model
AFT
AHe
Early (+2 Myr) Model
Late (-2 Myr) Model
Bobotogh thrust
Karshi thrust
Rangon thrust
Aruntau thrust
Jetimtau thrust
Karatau thrust
Sarsarak thrust
Sangyak Anticline
Vakhsh Anticline
NW
SE
C.
Elevation (km)
sample location
topography
Neogene
Yovon Valley
Eocene/ Paleocene
Oligocene
Late Cretaceous
Early Cretaceous
Jurassic
Paleozoic
Jurassic decollement
Paleozoic decollement
vertical exaggeration ≈ 2
10 km

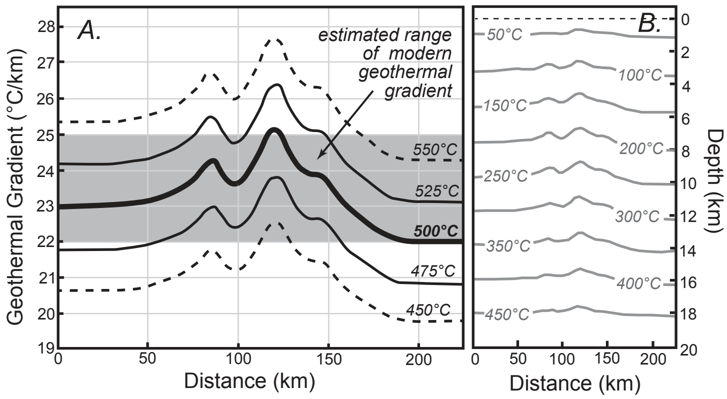
A.
estimated range of modern geothermal gradient
550°C
525°C
500°C
475°C
450°C
Geothermal Gradient (°C/km)
Distance (km)
B.
50°C
100°C
150°C
200°C
250°C
300°C
350°C
400°C
450°C
Depth (km)
Distance (km)

Figure 07

figure 08

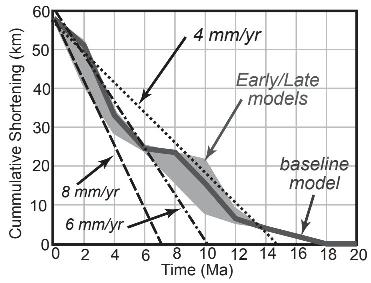

60
50
40
30
20
10
0
Cummulative Shortening (km)
0
2
4
6
8
10
12
14
16
18
20
Time (Ma)
4 mm/yr
Early/Late
models
baseline
model
8 mm/yr
6 mm/yr

Figure 09

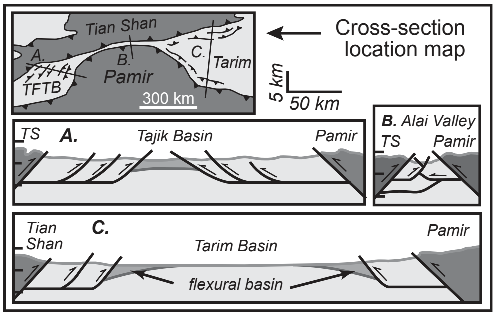
Cross-section location map
Tian Shan
A.
B.
C.
Tarim
Pamir
TFTB
300 km
5 km
50 km
TS
A.
Tajik Basin
Pamir
B. Alai Valley
TS
Pamir
Tian Shan
C.
Tarim Basin
Pamir
flexural basin

figure 10

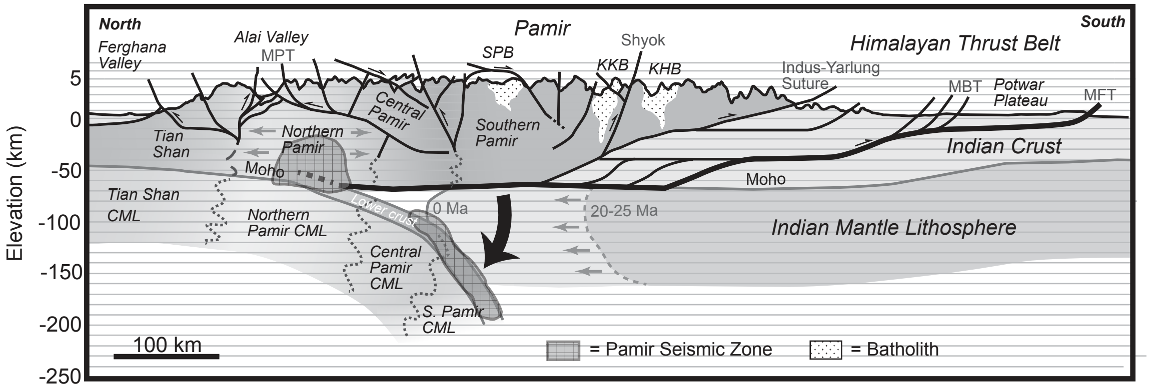
North
South
Pamir
Himalayan Thrust Belt
Ferghana Valley
Alai Valley
MPT
SPB
Shyok
KKB
KHB
Indus-Yarlung Suture
MBT
Potwar Plateau
MFT
Tian Shan
Northern Pamir
Central Pamir
Southern Pamir
Indian Crust
Moho
Tian Shan CML
Northern Pamir CML
Central Pamir CML
S. Pamir CML
Lower crust
0 Ma
20-25 Ma
Indian Mantle Lithosphere
Elevation (km)
5
0
-50
-100
-150
-200
-250
100 km
= Pamir Seismic Zone
= Batholith

Figure 11

Table 1. Sample Information

Sample Name	Sample Age	Latitude (°N)	Longitude (°E)	Elevation (m)	AHe Age (Ma)
IS-13-03	Late Cretaceous	38.477	68.551	957	3.0 ± 1.0
IS-13-01	Late Cretaceous	38.470	68.565	794	3.2 ± 1.4
IS-13-07	Neogene	38.445	68.595	1836	unreset
IS-13-04	Late Cretaceous	38.415	68.687	827	12.4 ± 4.6
IS-13-05	Late Cretaceous	38.194	68.600	1192	3.0 ± 1.2
14-11	Late Cretaceous	38.336	68.746	1270	9.0 ± 4.6
14-10	Late Cretaceous	38.108	68.606	780	3.1 ± 0.1
IS-13-06	Neogene	38.249	68.779	934	unreset
14-08	Late Cretaceous	38.391	69.065	1022	1.5 ± 0.9
14-07	Late Cretaceous	38.290	69.072	946	2.9 ± 0.8
14-05	Late Cretaceous	38.263	69.131	786	1.2 ± 0.4
SHSH-95	Late Cretaceous	38.356	69.253	1309	5.1 ± 1.6
14-03	Late Cretaceous	38.328	69.436	1146	6.7 ± 3.0
DS-13-08	Late Cretaceous	38.044	70.195	1252	4.2 ± 1.6
DS-13-01	Early Jurassic	38.253	68.565	2038	5.9 ± 4.1

#gr	AFT Age (Ma)
5	16.7 ± 4.1
5	
5	14.6 ± 2.9
5	
5	12.2 ± 2.5
4	
4	
5	5.6 ± 2.0
4	3.6 ± 1.1
5	<7
4	9.0 ± 2.6
4	
4	

Table 2. Model results for shortening in the Tajik Fold and Thrust Belt

Structure	Amount of slip (km) for each Time Step (Ma)									
	20-18	**18-16**	**16-14**	**14-12**	**12-10**	**10-8**	**8-6**	**6-4**	**4-2**	**2-0**
Bobotogh Thrust		2	2	1	1				4	3
Karshi Thrust				1.5	5	1.5				
Rangon Thrust					3	2.5				
Samol Thrust								2	4	
Dzhetymtau Thrust									4	3
Karatau Thrust							1	4	4	
Sarsarak Thrust								1	2	1
Sangyaak Fold								1.5		
Vakhsh Fold						4				
Total Slip for time step (km)	**0**	**2**	**2**	**2.5**	**9**	**8**	**1**	**8.5**	**18**	**7**

Total Slip on structure (km)
13
8
5.5
6
7
9
4
1.5
4
58